Discovery of novel arylpiperazine-based DA/5-HT modulators as potential antipsychotic agents – design, synthesis, structural studies and pharmacological profiling

Piotr Stępnicki[1*], Katarzyna M. Targowska-Duda[2], Antón L. Martínez[3,4], Agata Zięba[1], Olga Wronikowska-Denysiuk[5], Martyna Z. Wróbel[6], Agata Bartyzel[7], Alicja Trzpil[8], Tomasz M. Wróbel[1], Andrzej Chodkowski[6], Karolina Mirecka[6], Tadeusz Karcz[9], Katarzyna Szczepańska[9], Maria I. Loza[3,4], Barbara Budzyńska[5], Jadwiga Turło[6], Jadwiga Handzlik[9], Emilia Fornal[8], Ewa Poleszak[10], Marián Castro[3,4], Agnieszka A. Kaczor[1,11*]

[1]*Department of Synthesis and Chemical Technology of Pharmaceutical Substances, Faculty of Pharmacy, Medical University of Lublin, 4A Chodźki St., PL-20093 Lublin, Poland*

[2]*Department of Biopharmacy, Faculty of Pharmacy, Medical University of Lublin, 4A Chodźki St., PL-20093 Lublin, Poland*

[3]*Department of Pharmacology, Universidade de Santiago de Compostela, Center for Research in Molecular Medicine and Chronic Diseases (CIMUS), Avda de Barcelona, E-15782 Santiago de Compostela, Spain*

[4]*Instituto de Investigación Sanitaria de Santiago de Compostela (IDIS), Travesía da Choupana s/n, E-15706 Santiago de Compostela, Spain*

[5]*Independent Laboratory of Behavioral Studies, Chair of Biomedical Sciences, Faculty of Biomedicine, Medical University of Lublin, 4A Chodźki St., PL-20093 Lublin, Poland*

[6]*Department of Drug Technology and Pharmaceutical Biotechnology, Faculty of Pharmacy, Medical University of Warsaw, 1 Banacha Street, 02-097, Warszawa, Poland*

[7]*Department of General and Coordination Chemistry and Crystallography, Institute of Chemical Sciences, Faculty of Chemistry, Maria Curie-Sklodowska University in Lublin, Maria Curie-Sklodowska Sq. 2, 20-031 Lublin, Poland*

[8]*Department of Bioanalytics, Chair of Dietetics and Bioanalytics, Faculty of Biomedicine, Medical University of Lublin, Jaczewskiego 8b St., 20-090 Lublin, Poland*[9]*Department of Technology and Biotechnology of Drugs, Faculty of Pharmacy, Jagiellonian University, Medical College, Medyczna 9, PL-30-688 Kraków, Poland*

[10]*Chair and Department of Applied and Social Pharmacy, Faculty of Pharmacy, Medical University of Lublin, 1 Chodźki St., PL-20093 Lublin, Poland*

[11]*School of Pharmacy, University of Eastern Finland, P.O. Box 1627, FI-70211 Kuopio, Finland*

**Correspondence: piotrstepnicki93@gmail.com (P.S.), agnieszka.kaczor@umlub.pl (A.A.K.)*

Abstract: Schizophrenia is a mental disorder with a complex pathomechanism involving many neurotransmitter systems. Among the currently used antipsychotics, classical drugs acting as dopamine D_2 receptor antagonists, and drugs of a newer generation, the so-called atypical antipsychotics, can be distinguished. The latter are characterized by a multi-target profile of action, affecting, apart from the D_2 receptor, also serotonin receptors, in particular 5-HT_{2A} and 5-HT_{1A}. Such profile of action is considered superior in terms of both efficacy in treating symptoms and safety. In the search for new potential antipsychotics of such atypical receptor profile, an attempt was made to optimize the arylpiperazine based virtual hit, D2AAK3, which in previous studies displayed an affinity for D_2, 5-HT_{1A} and 5-HT_{2A} receptors, and showed antipsychotic activity *in vivo*. In this work, we present the design of D2AAK3 derivatives (**1** – **17**), their synthesis, and structural and pharmacological evaluation. The obtained compounds show affinities for the receptors of interest and their efficacy as antagonists/agonists towards them was confirmed in functional assays. For the selected compound **11**, detailed structural studies were carried out using molecular modeling and X-ray methods. Additionally, ADMET parameters and *in vivo* antipsychotic activity, as well as influence on memory and anxiety processes were evaluated in mice, which indicated good therapeutic potential and safety profile of the studied compound.

Keywords: antipsychotic, schizophrenia, multi-target compound, GPCR, arylpiperazine

Graphical abstract:

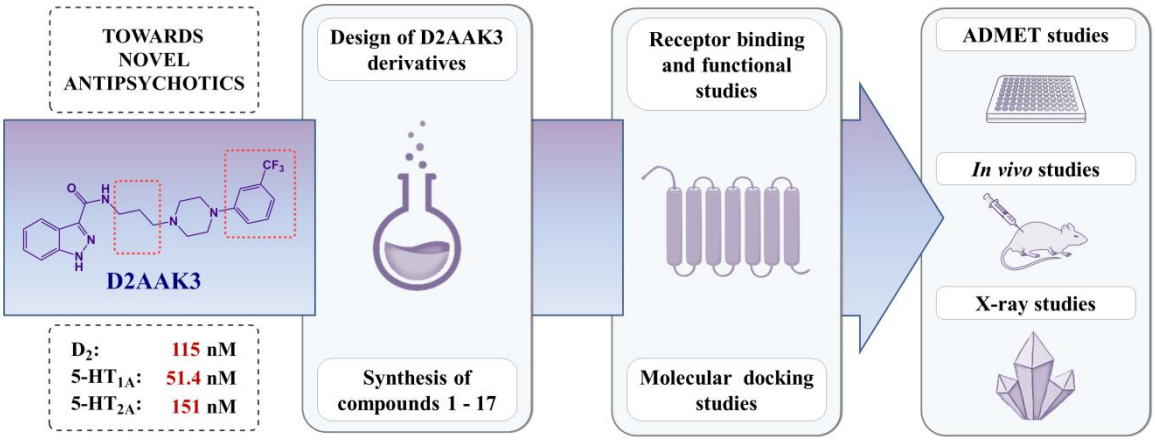

Highlights:

- Novel multi-target arylpiperazine-based ligands of aminergic GPCRs.
- Antagonists of D_2/5-HT_{2A} and agonists of 5-HT_{1A} receptors.
- Compound **11** shows antipsychotic activity *in vivo*.
- ADMET parameters of **11** confirm its beneficial pharmacokinetics.
- X-ray analysis of compound **11** reveals energetically stable conformation.

1. Introduction

Mental disorders are one of the most serious threats and challenges for clinical medicine, and due to the increasing risk of unfavorable factors, such as aging of the population, faster pace of life, migrations or conflicts, a further increase in their prevalence should be expected. One of the most severe psychiatric syndromes is schizophrenia, a chronic disease characterized by inadequate perception, assessment and reception of reality, impaired realistic assessment of the environment, oneself and relationships with others. The clinical picture of schizophrenia consists of symptoms that fall into three main categories: the so-called positive symptoms in the form of delusions and hallucinations; negative symptoms, such as disorganized thinking and affect, social withdrawal, reduced motivation; and cognitive deficits, which include memory disorders, impaired speed of thought processing or executive functions. According to estimates, about one in a hundred people may be affected by schizophrenia, and the disease itself is listed among the ten main causes of disability in the world [1,2].

In people suffering from schizophrenia, reduced physiological activity in the prefrontal cortex, temporal lobe, hippocampus, thalamus and cerebellum, as well as functional communication disorders between these structures are observed [3]. The currently dominant neurochemical model of schizophrenia, the dopaminergic hypothesis, is based on the fact that drugs that are antagonists of dopamine receptors, in particular the D_2 receptor, show antipsychotic properties [4]. The effectiveness of these drugs suggests that the increase in dopaminergic activity is associated with the pathomechanism of schizophrenia.

Despite the complex pathophysiology of schizophrenia, in which, apart from dopamine, neurotransmitters such as glutamate, GABA or serotonin are involved, most antipsychotic drugs developed so far, act as antagonists of the dopamine D_2 receptor. These drugs are especially effective in reducing positive and to some extent negative symptoms [5], but their use is

associated with the risk of serious side effects, especially extrapyramidal symptoms, dystonia, akathisia and drug-induced sedation [6,7]. A major problem associated with the use of antipsychotic drugs is also the generally poor clinical response of patients to pharmacological treatment [8,9]. A breakthrough in the treatment of schizophrenia symptoms was the introduction of clozapine, which is 30-40% effective in treating patients who meet the strict criteria of treatment resistance [10,11]. In addition, clozapine, compared to older-generation drugs, does not cause parkinsonism and dystonia, although its clinical use is limited by the risk of severe adverse reaction, agranulocytosis [12]. This drug gave rise to the second generation of antipsychotics, the so-called atypical drugs, the action of which is based mainly on the interaction with serotonin receptors, in particular on the blockade of the 5-HT_{2A} receptor, with maintained but reduced affinity for the dopamine D_2 receptor [13,14]. However, despite the superior efficacy of the second-generation prototype drug, clozapine, current atypical antipsychotics as a whole, generally show only slightly better efficacy compared to classical drugs, and none of them resulted as effective as clozapine [15]. Although atypical drugs carry the risk of causing side effects, especially weight gain and metabolic disorders, their undoubted advantage is the significantly reduced risk of the above-mentioned serious extrapyramidal adverse reactions that were associated to uncompensated D_2 blockade by first-generation drugs [12,16].

Considering the difficult issues related to schizophrenia, such as the complexity of its pathomechanism, frequent treatment resistance, low effectiveness of currently available drugs, especially in relation to the treatment of negative symptoms and cognitive disorders, and predictions according to which the incidence of this disease will increase, there is a need to develop new, more effective and safer drugs.

In light of the above, in the present study we focused on the search for new potential candidates for antipsychotic drugs that would show a multi-target mode of action. As in the

case of atypical neuroleptics, targeting several receptors simultaneously may be associated with certain benefits in terms of the drug's clinical efficacy and the safety profile compared to the classic first-generation, selective antipsychotics. In our previous work we reported a virtual hit, compound D2AAK3, which is a multi-target ligand for dopamine and serotonin receptors, in particular D_2, 5-HT_{1A} and 5-HT_{2A} receptors (Fig.1). Its further pharmacological evaluation revealed that it acts as antagonist of D_2 and 5-HT_{2A} receptors and agonist of 5-HT_{1A} receptor. Moreover, in behavioral studies in mouse models, it reduced amphetamine-induced hyperactivity and improved memory consolidation, but had a negative effect on anxiety processes, causing anxiety-producing effects 30 minutes after acute administration [17]. Considering these promising properties of D2AAK3 as a candidate lead structure, we decided to carry out its optimization campaign, aimed at obtaining compounds with a more favorable receptor profile, in particular with increased affinity for serotonin receptors, while retaining or reducing affinity for the dopamine D_2 receptor. The designed modifications of the D2AAK3 compound are schematically shown in Fig. 1, and they include the extension of the linker connecting the two distal fragments of the molecule by one carbon unit, and the replacement of the aromatic substituent in the arylpiperazine system. Here we present the synthesis of the designed derivatives, their structural characterization using molecular modeling and X-ray studies, and *in vitro* and *in vivo* evaluation of their pharmacological activity.

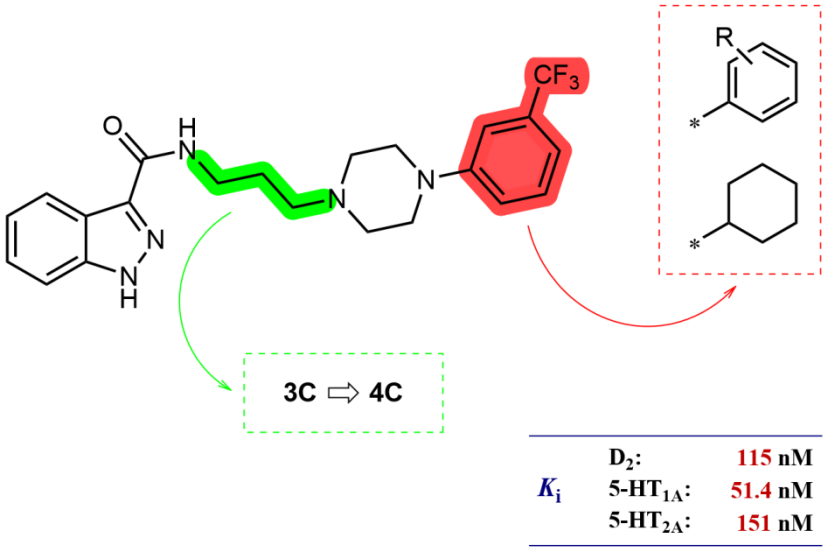

Fig. 1. Chemical formula of D2AAK3 with indicated designed structural modifications.

2. Results and discussion

2.1. Chemistry

The designed compounds (**1** – **17**) were obtained according to the synthetic route shown in Scheme 1. First, the Gabriel synthesis was applied as a convenient method to obtain primary aliphatic amines, which were then reacted with indazole-3-carboxylic acid, using 1,1'-carbonyldiimidazole (CDI) as a coupling agent, to obtain the final amides. The piperazines used to synthesize the intermediate compounds **1b** – **17b** and which were not commercially available, namely 3-fluoro, 2-chloro and 2-ethoxy phenylpiperazines (**I** – **III**), were obtained according to previously described methods [18,19] (Scheme 1).

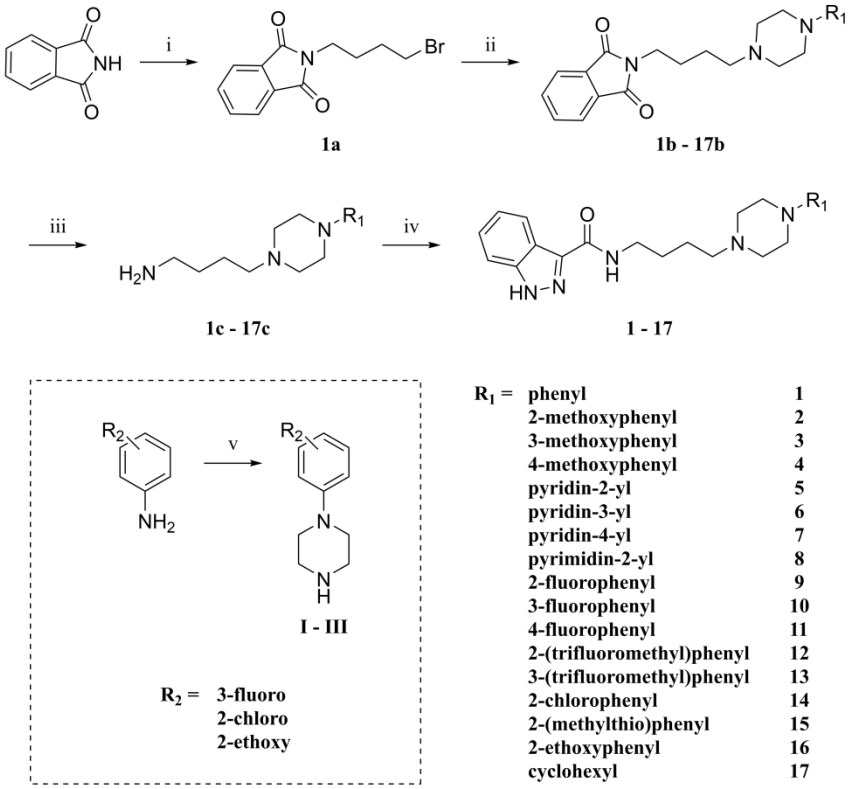

Scheme 1. Synthetic pathway for compounds **1 – 17** and **I – III**. Reagents and conditions: (i) 1,4-dibromobutane, K_2CO_3, butan-2-one, reflux, 10h; yield: 74%; (ii) *N*-substituted piperazine, K_2CO_3, $KI_{(cat.)}$, ACN, reflux, 5-22h; yield: 82-98%; (iii) $NH_2NH_2 \cdot H_2O$, EtOH 96%, reflux, 3h; yield: 40-95%; (iv) 1*H*-indazole-3-carboxylic acid, CDI, DMF, 60 °C, 2h → 4.5h; yield: 25-59%; (v) bis(2-chloroethyl)amine hydrochloride, diethylene glycol monomethyl ether, 150 °C, 16h; yield: 45-58%.

2.2. Affinity of compounds at the receptors of interest

Affinity of the compounds was evaluated at three receptor targets of interest, human dopamine D_2, serotonin 5-HT_{1A}, and serotonin 5-HT_{2A} receptors. Compounds were initially screened in competition radioligand binding assays at the single concentration of 10 μM, in membranes from stable cell lines heterologously expressing the cloned human receptors. Those compounds showing % of inhibition of the specific radioligand binding over 65% in these assays were assayed at typically six concentrations (from 10^{-10} or 10^{-9} M to 10^{-5} or 10^{-4} M) in

competition binding curves for determination of their affinity (equilibrium dissociation constant, K_i). Results, expressed as affinity value (K_i, [nM]) or as % of inhibition of specific radioligand binding at 10 μM compound concentration (% inh.), are given in Table 1. All the compounds for which affinity values are given fully displaced specific radioligand binding in a concentration-dependent manner at the three receptors assayed. The competition radioligand binding curves for reported compounds at D_2, 5-HT_{1A}, and 5-HT_{2A} receptors, as well as for the corresponding reference standard haloperidol (D_2), 5-carboxamidotryptamine (5-CT) (5-HT_{1A}), and risperidone (5-HT_{2A}) may be found in Supplementary Information (Fig. S1, S2 and S3). Three compounds (**3**, **4**, and **11**) representative of the series were selected based on affinity profiles, in particular 5-HT_{2A}/D_2 affinity ratio in comparison to the D2AAK3 compound, for further selectivity profiling and investigation of their efficacy at the receptors of interest.

Table 1. Competitive radioligand binding data at human D_2, 5-HT_{1A} and 5-HT_{2A} receptors. Data are expressed as % inh. at 10 μM, or K_i (nM) when full displacement was achieved (mean ± SEM of 2-5 for D_2, 2-3 for 5-HT_{1A} or 2-4 for 5-HT_{2A} independent experiments performed in duplicate).

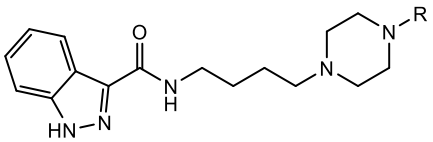

Compound	R	D_2	5-HT_{1A}	5-HT_{2A}
1	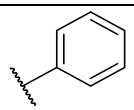	69.7 ± 7.9	25.6 ± 4.1	135 ± 7
2	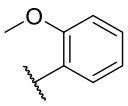	8.71 ± 0.37	4.84 ± 0.46	321 ± 26
3	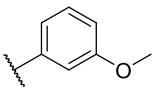	108 ± 13	20.7 ± 2.0	128 ± 20
4	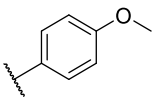	62.0 ± 1.7%	826 ± 7	706 ± 44

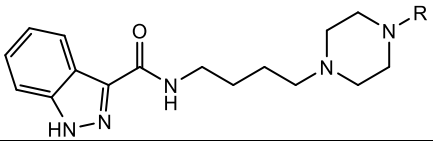

	R			
5	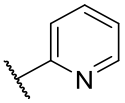	239 ± 22	37.2 ± 2.1	401 ± 20
6	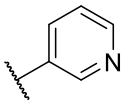	557 ± 64	405 ± 83	40.1 ± 5.4%
7	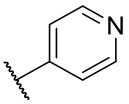	10.0 ± 2.2%	33.3 ± 3.9%	16.4 ± 10.3%
8	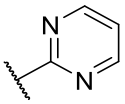	264 ± 23	139 ± 16	2917 ± 377
9	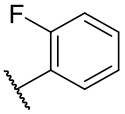	26.4 ± 0.5	29.0 ± 3.8	184 ± 16
10	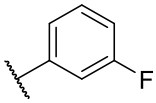	76.4 ± 9.2	33.3 ± 3.0	243 ± 3
11	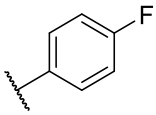	596 ± 91	56.6 ± 5.2	66.7 ± 11.2
12	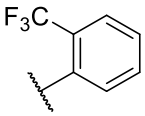	8.57 ± 1.59	114 ± 36	1189 ± 152
13	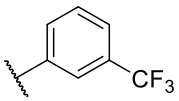	109 ± 6	14.0 ± 0.6	171 ± 18
14	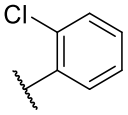	11.8 ± 1.2	23.0 ± 4.4	144 ± 17
15	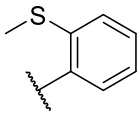	9.93 ± 1.89	4.07 ± 0.56	179 ± 6
16	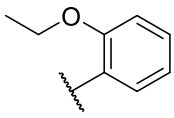	9.86 ± 0.99	6.47 ± 0.66	318 ± 5
17	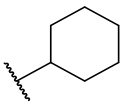	26.7 ± 9.3%	43.4 ± 1.0%	52.6 ± 6.6%
D2AAK3		115 ± 15	51.4 ± 18.4	151 ± 73
Haloperidol		7.41 ± 0.87 (n=11)		

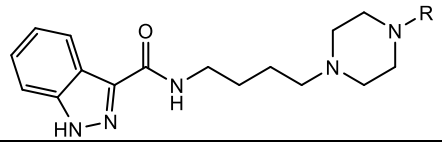

5-CT	0.26 ± 0.04 (n=5)	
Risperidone		0.23 ± 0.02 (n=5)

2.3. Selectivity of selected compounds at secondary targets

The selectivity of compounds **3**, **4**, and **11** was evaluated at serotonin 5-HT_{2C}, histamine H_1 and muscarinic M_1 receptors (Table 2). Only compound **3** displayed affinity at histamine H_1 receptor in the medium nanomolar range (K_i = 76.4 nM) and at serotonin 5-HT_{2C} receptor in the medium to high nanomolar range (K_i = 114 nM), whereas none of the three selected compounds displayed affinity for muscarinic M_1 receptor. Considering that these receptors are antitargets in schizophrenia and interaction with them may lead to the occurrence of adverse effects, the lack of affinity of the tested compounds for these receptors (except for compound **3** for the H_1 receptor) is a beneficial property, as it may improve a safety profile of the studied compounds.

Table 2. Competitive radioligand binding data for compounds **3**, **4** and **11** at human 5-HT_{2C}, H_1 and M_1 receptors. Data (mean ± SEM of 2 independent experiments performed in duplicate) are expressed as % inh. at 10 μM or K_i (nM).

Compound	5-HT_{2C}	H_1	M_1
3	114 ± 14	76.4 ± 5.8	10 ± 5%
4	1816 ± 390	1303 ± 535	6 ± 1%
11	552 ± 68	1140 ± 291	0%
Risperidone	2.43 ± 0.15		
Doxepin		0.86 ± 0.15	
Ipratropium			2.11 ± 0.02

2.4. Efficacy of selected compounds in cell-based assays of receptor signaling

The efficacy as agonists or antagonists of the three selected compounds **3**, **4**, and **11** was investigated at the three receptors of interest in cell-based functional assays of second messenger production. Assays were carried out in the same stable cell lines expressing the human receptors employed in radioligand binding assays. Specifically, dopamine D_2 and serotonin 5-HT_{1A} receptor signaling was assessed as inhibition of forskolin-stimulated cAMP production, and serotonin 5-HT_{2A} receptor signaling was assessed as stimulation of inositol phosphate (IP) production. Compounds were tested at maximal concentration of 10^{-5} M to avoid interferences of vehicle in these cell-based assays, and concentration-response curves were carried out for the two compounds with the highest receptor affinities (**3** and **11**) (Fig. 2).

Compounds **3**, **4**, and **11** antagonized the inhibition of forskolin-stimulated cAMP production elicited by 10^{-6} M dopamine in CHO-K1 cells stably expressing human D_2 receptors, indicative of D_2 antagonistic activity (Fig. 2A, Table 3). With the limitation that none of the three selected compounds achieved full antagonism of dopamine response at the highest compound concentration assayed (10^{-5} M), the three compounds preserved a rank of potency and efficacy in agreement with their affinities for D_2 receptor (**3** > **11** > **4**), with compounds **3** and **11** showing a potency of $K_b \approx 8.11$ nM and ≈ 45.7 nM, respectively, as estimated from inhibition concentration–response curves of the compounds against a single agonist concentration of 10^{-6} M.

As for serotonin receptors, compounds **3**, **4**, and **11** inhibited the forskolin-stimulated cAMP production in HEK293 cells stably expressing 5-HT_{1A} receptors in a concentration-dependent manner (Fig. 2B, Table 3), indicative of 5-HT_{1A} agonistic activity, while they behaved as 5-HT_{2A} antagonists, antagonizing the inositol phosphate production stimulated by 10^{-6} 5-HT in CHO-K1 cells expressing 5-HT_{2A} receptors (Fig. 2C, Table 3). Compounds displayed a rank of potencies in functional assays at serotonin receptors in agreement with their

corresponding receptor affinities (**3** > **11** at 5-HT_{1A}, **11** > **3** at 5-HT_{2A}). Therefore, the selected compounds displayed D_2/5-HT_{2A} antagonist combined with 5-HT_{1A} agonist profile.

Table 3. Potency and efficacy of selected compounds at D_2, 5-HT_{1A}, and 5-HT_{2A} receptor signaling. Compounds were evaluated in cell-based functional assays of second messenger production (inhibition of forskolin-stimulated cAMP signaling for D_2 and 5-HT_{1A} receptors, stimulation of IP production for 5-HT_{2A} receptors) in cell lines stably overexpressing the human receptors. D_2 antagonistic activity of the compounds was quantified as inhibition of 1 µM dopamine (DA) response; 5-HT_{1A} agonistic activity was quantified as inhibition of 1 µM forskolin (FSK)-stimulated cAMP production, and 5-HT_{2A} antagonistic activity was quantified as inhibition of 1 µM serotonin (5-HT) response. The table shows potency values, expressed as pK_b (-logK_b) and K_b (nM) for antagonists and as pEC_{50} (-logEC_{50}) and EC_{50} (nM) for agonists, as well as efficacy values at 10 µM concentration of the compounds, expressed as % of inhibition (%inh.) of the indicated response. K_b values of antagonists were calculated from the inhibition concentration–response curves of the compounds against a single agonist concentration of 10^{-6} M. Average EC_{50} values for DA and 5-HT in these assays were 116 nM and 569 nM (pEC_{50} DA (mean ± SEM) = 6.94 ± 0.16; pEC_{50} 5-HT (mean ± SEM) = 6.25 ± 0.06). Data shown in the table are mean ± SEM of 2-3 (D_2, 5-HT_{1A}) or 2-4 (5-HT_{2A}) independent experiments performed in duplicate. n.d., not determined.

Compound	D_2 antagonism (cAMP signaling)			5-HT_{1A} agonism (cAMP signaling)			5-HT_{2A} antagonism (IP signaling)		
	pK_b	K_b (nM)	%inh. of DA response	pEC_{50}	EC_{50} (nM)	%inh. of FSK response	pK_b	K_b (nM)	%inh. of 5-HT response
3	8.09 ± 0.11	8.11	64.6 ± 7.0%	7.55 ± 0.09	28.4	84.4 ± 3.2%	6.79 ± 0.05	163	93.4 ± 2.1%
4	n.d.	n.d.	24.2 ± 2.0%	n.d.	n.d.	44.3 ± 3.5%	n.d.	n.d.	63.9 ± 5.6%
11	7.34 ± 0.12	45.7	56.4 ± 14.6%	6.80 ± 0.07	160	81.0 ± 4.8%	7.02 ± 0.17	96.4	75.4 ± 5.6%

Compound	D_2 antagonism (cAMP signaling)			$5\text{-}HT_{1A}$ agonism (cAMP signaling)			$5\text{-}HT_{2A}$ antagonism (IP signaling)		
	pK_b	K_b (nM)	%inh. of DA response	pEC_{50}	EC_{50} (nM)	%inh. of FSK response	pK_b	K_b (nM)	%inh. of 5-HT response
Haloperidol	9.53 ± 0.07	0.29	92.1 ± 0.6%	n.d.	n.d.	n.d.	n.d.	n.d.	n.d.
5-CT	n.d.	n.d.	n.d.	9.57 ± 0.19	0.27	95.3 ± 6.0%	n.d.	n.d.	n.d.
Risperidone	n.d.	n.d.	n.d.	n.d.	n.d.	n.d.	9.77 ± 0.09	0.17	104.5 ± 1.3%

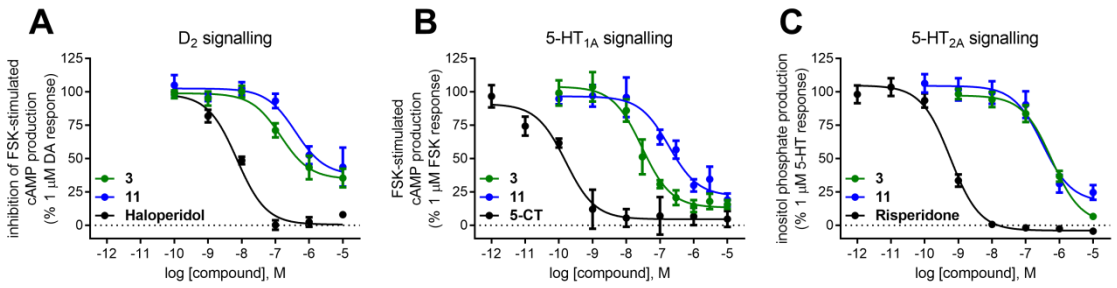

Fig. 2. Concentration-response curves of compounds **3**, **11**, and reference ligands haloperidol (as D_2 antagonist), 5-CT (as $5\text{-}HT_{1A}$ agonist), and risperidone (as $5\text{-}HT_{2A}$ antagonist) in functional assays of cAMP signaling (D_2, $5\text{-}HT_{1A}$) and IP production ($5\text{-}HT_{2A}$). Data are expressed as % of 1 µM dopamine (DA) response (A), % of 1 µM forskolin (FSK)-stimulated cAMP production (B), and % of 1 µM serotonin (5-HT) response (C). The graph shows data (mean ± SEM) of 2-3 (D_2, $5\text{-}HT_{1A}$) or 2-4 ($5\text{-}HT_{2A}$) independent experiments performed in duplicate.

2.5. Structure-activity relationship

One of the objectives of the research was to investigate the effect of various substituents, mostly aryl groups, in the 4-position of the piperazine, with the simultaneous extension of the carbon linker between the amide group and piperazine to four methylene groups, on the activity of the obtained compounds towards the D_2, $5\text{-}HT_{1A}$ and $5\text{-}HT_{2A}$ receptors.

In the case of the dopamine D_2 receptor, the influence of the position of the substituent on the phenyl group attached to the piperazine on the activity of a given compound is evident. The most active are derivatives containing an *ortho*-substituted phenyl group, with affinities ranging from 8.57 to 26.4 nM. Among them, the size of the substituent seems to affect the binding affinity the most – the trifluoromethyl group and ether substituents show greater activity than halogen substituents. However, the differences are rather subtle. Next in terms of activity are *meta*-substituted phenyls and in this group the trend seems to be opposite to that of the more active *ortho*-substituted derivatives. Namely, the fluorine atom introduced in this position increases the activity compared to the larger substituents – trifluoromethyl and methoxy. The unsubstituted phenyl group, in turn, resides between compounds with *ortho* and *meta* substituted phenyl groups in terms of binding affinity, but exhibits more *meta*-like activity than *ortho*-substituted phenyls. In the series of activities of the tested derivatives at the D_2 receptor, next are compounds with nitrogen-containing aryl system. Again, the above tendency is maintained – compounds with nitrogen atom replacing carbon adjacent to C1 – pyridin-2-yl and pyrimidin-2-yl substituents – show about twice higher binding affinity than the pyridin-3-yl substituent. Introducing a substituent at the 4-position of the phenyl leads to an even greater drop in activity, with larger substituents being less preferred. Also in the case of compounds with a replaced carbon atom, the 4-position is the least preferred, resulting in a complete loss of activity. Moreover, the installation of an alicyclic substituent instead of an aryl is associated with the lack of activity of a given compound.

As for the activities of the obtained compounds at the 5-HT_{1A} serotonin receptor, the general trend is similar to the activity at the D_2 receptor. The derivatives having the highest binding affinity are those possessing an ether or thioether substituent in the *ortho* position of the phenyl ring. Electron-withdrawing groups at this position, such as halogens and the trifluoromethyl group, appear to reduce activity. The stronger the electron-withdrawing effect

of a substituent, the lower the activity of that derivative. The opposite tendency occurs for compounds with *meta*-substituted phenyl moieties. The strongest electron-withdrawing substituent, trifluoromethyl, produces the highest activity. The size of the substituent at this position on the phenyl ring can also influence the binding affinity – larger substituents appear to be more preferred. However, this dependency does not translate into a significant spread in the binding affinities of the compounds, which are in the range of 14.0 to 33.3 nM. As with the D_2 receptor, derivatives containing a *para*-substituted phenyl group show less activity compared to *ortho* and *meta* substitutions, and here again, the introduction of a larger, methoxy substituent leads to a greater decrease in activity. A similar influence of the position of the introduced modification on the activity can be noticed in the case of the replacement of the carbon atom in the phenyl ring with the nitrogen atom. While these modifications are generally less favorable in terms of activity than the preservation of the phenyl ring, among them also the derivatives having exchanged C2 and C6, that is pyridin-2-yl and pyrimidin-2-yl, followed by pyridin-3-yl, show the greatest affinity. The pyridin-4-yl derivative, as in the case of the D_2 receptor, is not active. The same is the case with the cyclohexyl derivative.

The structure-activity relationship toward 5-HT_{2A} receptor does not form a clear pattern as with the D_2 and 5-HT_{1A} receptors. The compound containing the *para*-fluorophenyl substituent shows the greatest activity – its binding affinity is almost twice as high as that of the second most active derivative, *meta*-methoxyphenyl. On the other hand, a compound containing a methoxy group at the para position of the phenyl ring exhibits one of the lower activities, which may indicate that the size of the substituent at that position is a key factor influencing binding to the receptor. Compounds with unsubstituted phenyl or *ortho* and *meta* substituted phenyl show comparable binding affinities in the range of 128 to 321 nM. Among compounds with *ortho* and *meta* substitutions, only the trifluoromethyl group shows a large, almost sevenfold dispersion in binding affinities depending on the location of the substituent,

with the *ortho* position being less preferred. The replacement of carbon with nitrogen in the phenyl ring is not favorable, leading to compounds with very little or no activity. Only the pyridin-2-yl derivative shows moderate activity with a binding affinity of 401 nM. As before, the aryl substituent at the 4-position of the piperazine turns out to be an essential element for binding to the 5-HT_{2A} receptor and replacing it with an alicyclic substituent leads to a loss of activity.

Considering the influence of the length of the linker connecting the two distal parts of the obtained compounds on their activity, it can be concluded that its extension by one methylene group does not significantly affect the binding to the D_2 and 5-HT_{2A} receptors. Both compound **13** and virtual hit D2AAK3 show very similar binding affinities for these receptors (109 nM vs. 115 nM for D_2 and 171 nM vs. 151 nM for 5-HT_{2A}). However, in the case of the 5-HT_{1A} receptor, introducing such modification appears to improve binding affinity by more than threefold (14.0 nM vs. 51.4 nM).

2.6. Molecular modeling

In order to study the interactions of the designed compounds with the target receptors at the molecular level, the molecular docking technique was used. Compounds **1**-**17** were docked to the orthosteric binding sites of the dopamine D_2 receptor and serotonin 5-HT_{2A} receptor crystal structures in the inactive state, and the serotonin 5-HT_{1A} receptor in the active state. The conformations of the receptors were chosen based on the results of functional studies, which indicated that the selected compounds are D_2 and 5-HT_{2A} receptor antagonists and 5-HT_{1A} receptor agonists. The interactions of the representative compound **11**, which was selected for further evaluation, with the above-mentioned receptors are shown in Figure 3. In each case, the main interaction of the ligand with the binding pocket of the protein is the electrostatic interaction of the protonatable nitrogen atom in the piperazine system of the ligand with the

conserved Asp 3.32 of the protein (Ballesteros-Weinstein numbering [20]). This is consistent with the classical pharmacophore model for aminergic GPCRs.

In the case of the D_2 receptor, apart from the interaction with Asp 3.32, additional interactions stabilizing the ligand in the binding pocket are mainly π-π stacking interactions of the aromatic systems of the ligand with the side chains of aromatic amino acids, more specifically: interactions between the benzene ring in the indazole group with Trp 7.40 and the phenyl ring at the piperazine system with aromatic parts of Phe 6.52 and Trp 6.48. In addition, a hydrogen bond is formed between the indazole NH and the hydroxyl group in the side chain of Ser 7.36. π-π stacking interactions can also be distinguished among the interactions of compound **11** with the orthosteric site of the 5-HT_{1A} receptor – the indazole moiety interacts in this manner with Tyr 2.64 on the second transmembrane helix (TM2), while the aryl part of piperazine interacts with Phe 6.52 on the sixth transmembrane helix (TM6). In the case of the 5-HT_{2A} receptor, as in the D_2 receptor, the 4-fluorophenyl group interacts with the aromatic systems of Phe 6.52 and Trp 6.48 via π-π stacking. Additionally, there is a hydrogen bond between the NH of the indazole and the amide carbonyl group of Asn 7.36.

For the D_2 receptor, most of the **1** – **17** compounds adopt similar docking poses, with the indazole part facing the extracellular side of the receptor and the arylpiperazine moiety located deeper in the binding site. This is also in line with previously reported docking conformation of the D2AAK3 compound [17]. Based on the Glide scoring function only compounds with meta- and para-methoxyphenyl substituents show an inverse position in the binding pocket, with indazole moiety directed inside the receptor. In the case of the 5-HT_{1A} receptor, all docked compounds are arranged similarly at the binding site, forming a "boat" shape, with the distal fragments of the molecule, that is indazole and phenyl group, facing outwards, and the central piperazine and carbon linker part bending deeper into the binding pocket. This is different from D2AAK3, which in 5-HT_{1A} receptor adopts a pose parallel to the

helices, thus similar to the D_2 receptor [17]. This difference may be due to D2AAK3 having a carbon linker shorter by one methylene unit, which may allow the ligand to penetrate deeper into the binding pocket. It is also in line with affinity studies which indicate that compound **13**, which differs from D2AAK3 only in the length of the linker, has about three times greater affinity for the 5-HT_{1A} receptor. This indicates the importance of the length of the carbon spacer on the assumed conformation of the ligand in the binding pocket and on its affinity for the 5-HT_{1A} receptor. In the case of the 5-HT_{2A} receptor, the docking results indicate less consistency in the conformation adopted at the binding site by the studied compounds. In general, compounds with an *ortho* or *para*-substituted phenyl group are most likely to assume a pose with the indazole group facing the outside of the receptor, while the *meta*-substituted compounds and compounds in which at least one carbon atom in the phenyl group has been replaced with nitrogen, align the opposite way, with the arylpiperazine group facing the extracellular space.

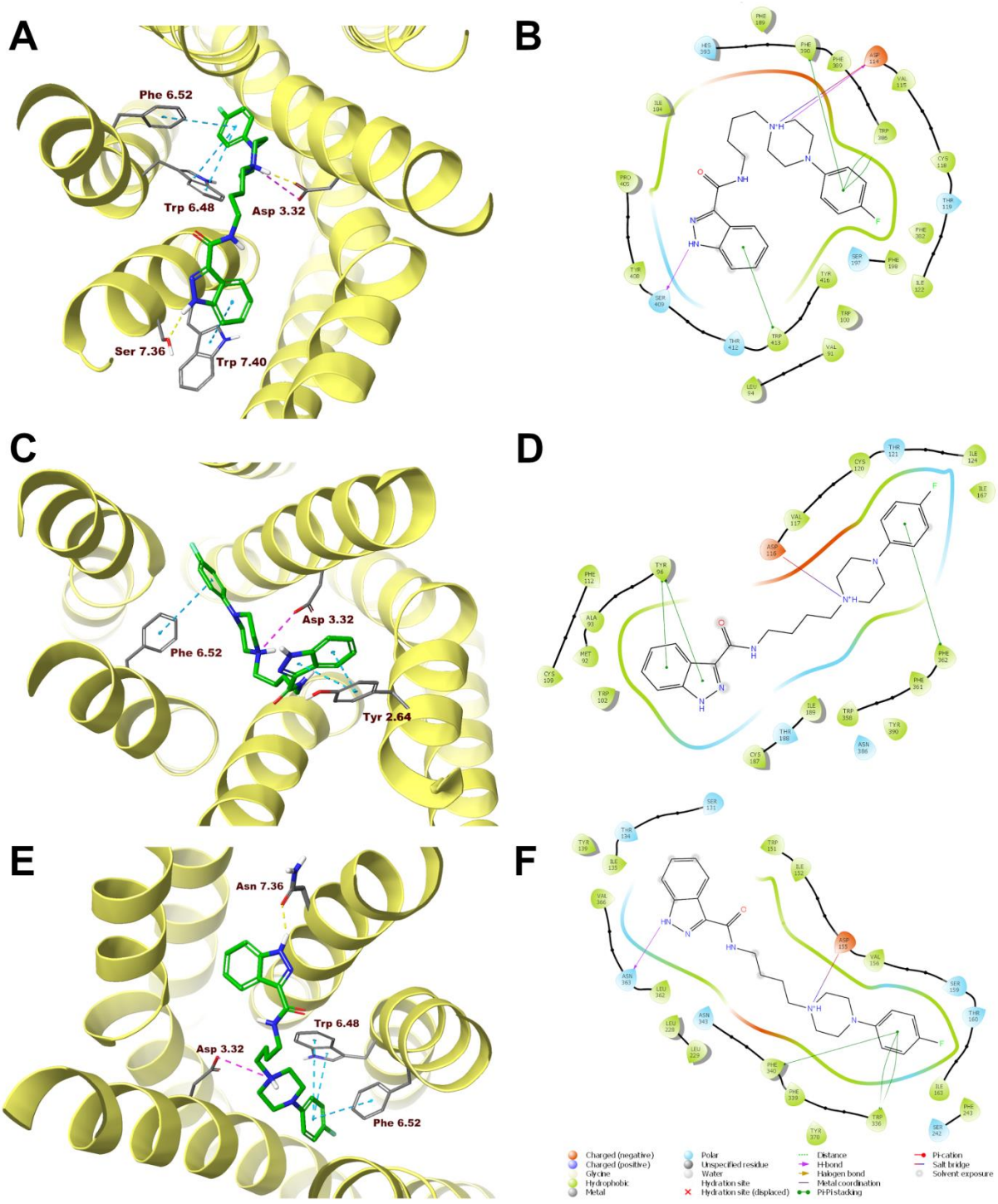

Fig. 3. Compound **11** in the binding pockets of human dopamine D_2 (A, B), serotonin 5-HT_{1A} (C, D) and serotonin 5-HT_{2A} (E, F) receptors. A, C, E – 3D view of the binding site. Ligand is represented as sticks with green carbon atoms. Protein is represented as yellow ribbons, main interacting residues are shown as sticks with grey carbon atoms. Electrostatic interactions are shown as pink dashed lines, hydrogen bonds as yellow dashed lines, π-π stacking as light blue

dashed lines. Non-polar hydrogen atoms were omitted for clarity. B, D, F – 2D view of the binding sites.

2.7. X-ray studies

The results of X-ray analysis are presented in Figure 4, and Figures S4, S5 and S6 in Supplementary Information, and in Table 4, and Tables S1 and S2 in Supplementary Information. A survey of the Cambridge Structural Database (CSD version 2022.2.0 with updates September 2022 [21] revealed that there is no similar compound building with the *N*-substituted 1*H*-indazole-3-carboxamide and 1-(4-fluorophenyl)piperazine units. Compound **11** crystallizes in the centrosymmetric triclinic space group $P\bar{1}$ with two independent molecules (A and B, Fig. 4) in the asymmetric unit. Both molecules are non-planar. Bond distances and angles are in the expected ranges [22] and agree with values observed for compounds containing the relevant building units [23–28]. The molecules A and B are connected *via* N-H···O hydrogen bond forming infinite $C_2^2(12)$ chains structure (Fig. S4A) [29]. As expected, the indazole moieties are planar (r.m.s. atomic displacement for the nonhydrogen atoms is 0.017 for A and 0.007 for B molecules) with a maximum deviation of -0.026(1) Å of N(1) for A and -0.009(2) Å of C24 for B atoms from the best plane. The carboxamide group is roughly coplanar with the indazole scaffold (dihedral angle equal 9.2(1)° for A and 5.2(2)° for B molecules). The mean plane formed by the nonhydrogen atoms of 1*H*-indazole-3-carboxamide moieties is almost orthogonal to the mean plane of the 1-(4-fluorophenyl)piperazine units, dihedral angles are equal to 85.69(3) Å for A and 85.16(3) Å for B molecules. The piperazine rings adopt distorted chair conformation, with puckering amplitude Q = 0.564(2)°, θ = 175.4(2)°, φ = 178.0(2)° for A and Q = 0.546(2)°, θ = 7.4(2)°, φ = 6.6(2)° for B molecules [30–32].

As mentioned above, the presence of N–H···O hydrogen bonds joins the molecules into infinite chains propagated along [001] direction (Fig. S4B). As can be seen in Fig. S5, these

chains are linked via C(19)-H(19)···F(2) hydrogen bonds in ribbons. The formed ribbons are further bound by C(19)-H(19)···F(2) and C(19)-H(19)···F(2) hydrogen bonds into a double layer (Fig. S6).

Table 4. Hydrogen bonding geometry [Å, º] for compound **11**.

D-H···A	d(D-H)	d (H···A)	d(D···A)	∠ DHA
N(2)-H(2N)···O(2)	0.95(2)	1.802(19)	2.729(2)	166(2)
N(7)-H(7N)···O(1)^{i}	0.88(2)	1.931(19)	2.765(2)	157(2)
C(4)-H(4)···F(2)^{ii}	0.95	2.47	3.203(2)	134
C(19)-H(19)···F(2)^{iii}	0.95	2.48	3.277(2)	141
C(23)-H(26)···F(1)^{iv}	0.95	2.45	3.316(2)	152

Symmetry code: (i) x, y, z-1; (ii) x-1, y-1, z-1; (iii) -x+1,-y+3,-z+2; (iv)) x-1, y-1, z-2;

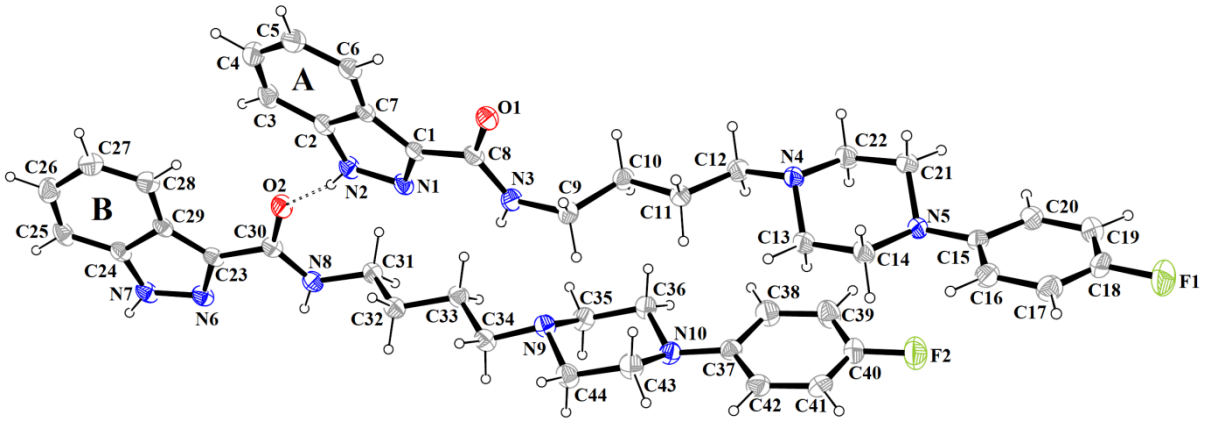

Fig. 4. A view of the asymmetric unit of **11** with displacement ellipsoids drawn at the 50% probability level.

2.8. ADMET parameters

2.8.1. Permeability profile

Parallel artificial membrane permeability assay (PAMPA) was used to test the potency of compound **11** to penetrate across lipid membranes. In this experimental setting, the ability of a compound to passively diffuse through a lipid-infused artificial membrane is being evaluated [33]. By application of UPLC-MS spectrometry the quantity of molecules penetrating

from donor to acceptor wells through phospholipid membrane was estimated. The results were expressed as permeability coefficient P_e calculated according to the formulas described in the literature [34]. The result obtained for **11** was compared to well-permeable Caffeine (P_e = 9.13×10^{-6} cm/s) and low-permeable Sulpiride (P_e = 0.00623×10^{-6} cm/s) (Table 5). Based on that comparison compound **11** was classified as showing moderate passive transport through biological membranes.

The ability to penetrate lipid membranes affects the pharmacokinetic profile of potential drug candidates, in particular oral-absorption, and is therefore one of the key parameters that should be determined at an early stage of drug development. Based on the results from the PAMPA assay, it may be predicted that permeability coefficient for compound **11** would translate into moderate/good absorption *in vivo*.

Table 5. PAMPA results (permeability coefficient P_e) for tested compounds.

Compound	P_e (10^{-6} cm/s)
11	1.81
Caffeine	9.13
Sulpiride	0.00623

2.8.2. Influence on cytochrome P450 3A4 activity

Compound **11** was additionally tested for its influence on CYP3A4 activity. Contrary to ketoconazole, a reference cytochrome P450 inhibitor, **11** caused significant, dose-dependent induction of enzyme activity (Fig. 5). The CYP3A subfamily of human cytochrome P450, to which the CYP3A4 enzyme belongs, is involved in the metabolism of approximately half of the drugs on the market [35]. Interfering with this enzyme by inhibiting or inducing it may lead to drug-drug interactions and thus unwanted adverse effects [36]. Compound **11** is a relatively

low potency CYP3A4 inducer, however, considering that many drugs, especially antipsychotics and antidepressants which are often taken by schizophrenic patients, are substrates of this enzyme, this issue should be addressed in the further optimization process.

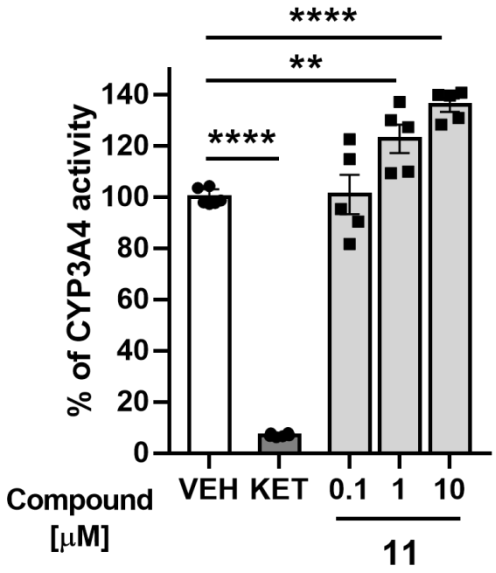

Fig. 5. Cytochrome CYP3A4-inducing activity of compound **11**. VEH, vehicle (0.25% DMSO); KET, Ketoconazole (10 μM). $^{**}p < 0.01$; $^{****}p < 0.0001$. Data were analyzed using one-way ANOVA followed by Dunnett's post hoc test.

2.8.3. Evaluation of neurotoxicity

To exclude potential neurotoxic activity, compound **11** was also tested for its influence on cell viability using 3-(4,5-dimethylthiazol-2-yl)-5-(3-carboxymethoxyphenyl)-2-(4-sulfophenyl)-2*H*-tetrazolium (MTS) assay and SH-SY5Y neuroblastoma cell line model. Clinical cytotoxic drugs: Doxorubicin and Paclitaxel were used as reference compounds inducing cell death. The investigated compound **11** represented good safety profile and showed significant cytotoxic activity only at 30 μM concentration (Fig. 6).

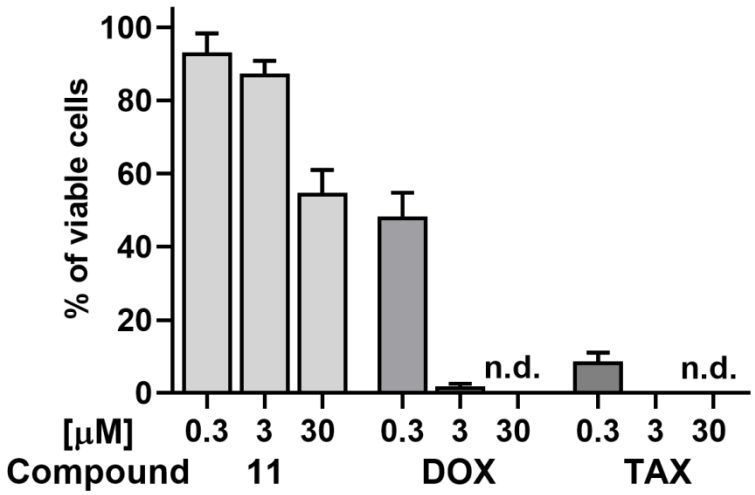

Fig. 6. SH-SY5Y cell viability after 72 hours incubation with the indicated compounds, examined using the CellTiter 96 AQueous nonradioactive cell proliferation assay. DOX, Doxorubicin; TAX, Paclitaxel; n.d., not determined.

2.8.4. Interaction with P-glycoprotein

Since interaction with the efflux transporters, including P-glycoprotein (P-gp), may limit the drug accumulation into the brain, compound **11** was tested for its activity towards that membrane protein. Influence on the ATPase activity of P-gp was tested to verify if **11** may be a substrate of P-glycoprotein. Tested at 20 μM concentration, **11** did not induce the energy consumption by recombinant protein suggesting a lack of P-gp substrate properties (Fig. 7). As for a potential drug candidate acting in the central nervous system, this feature may be considered advantageous as it prevents the compound from being removed from the brain, enabling it to reach the desired concentration.

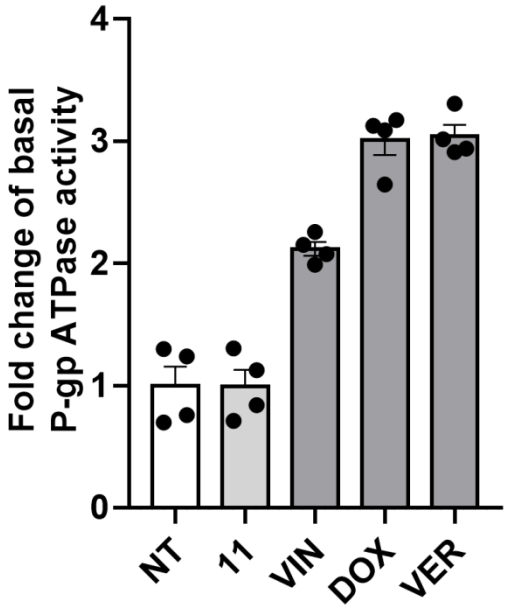

Fig. 7. Effect of compound **11** and reference P-gp substrates – Vincristine (VIN), Doxorubicin (DOX) and Verapamil (VER) on ATPase activity of P-glycoprotein. Compound **11**, VIN and DOX were tested at final concentration of 20 µM, whereas verapamil was used at 200 µM concentration. Data shown represent mean values ± SEM from two experiments conducted at least in duplicates.

2.8.5. *In vivo* PK/BBB permeability

The blood to plasma ratio provides information on the degree of binding of the compound to erythrocytes and is an important parameter in the evaluation of the pharmacokinetics of drug candidates. The experimentally determined value of the blood to plasma ratio for compound **11** is 1.02, indicating that it reached similar concentrations in whole blood and plasma, and thus binds to erythrocytes and plasma proteins to a similar extent. The maximum concentration of compound **11** in plasma was reached 60 min after administration (Table 6 and Fig. 8), which is consistent with subsequent behavioral studies and indicates an appropriately selected time from administration to testing in the experimental protocols used. In addition, the concentration of the tested compound in the brain at 30 and 60 min after

administration and the brain uptake at these time points were determined (Table 6). Concentration of compound **11** in the brain was found to be higher at 60 min than at 30 min. However, the influx constant (K_{in}), indicative of brain uptake, reached a higher value at 30 min than at 60 min, suggesting a decreasing permeability of compound **11** into the brain in this time interval.

Table 6. PK/BBB parameters of compound **11** in mice (n = 6) after ip administration of 40 mg/kg; data reported as mean values with standard deviations.

	5 min	**15 min**	**30 min**	**60 min**	**3 h**	**6 h**	**12 h**	**24 h**
Plasma concentration [ng mL^{-1}]	184 ± 45	202 ± 20	293 ± 33	308 ± 16	103 ± 11	41 ± 9	31 ± 6	22 ± 2
AUC_{T0} [min µg mL^{-1}]	0.46	2.39	6.10	15.12	39.82	52.84	65.78	84.53
Brain concentration [µg g^{-1}]			2.21 ± 0.56	2.93 ± 0.23				
K_{in} [mL min^{-1} g^{-1}]			0.363	0.194				

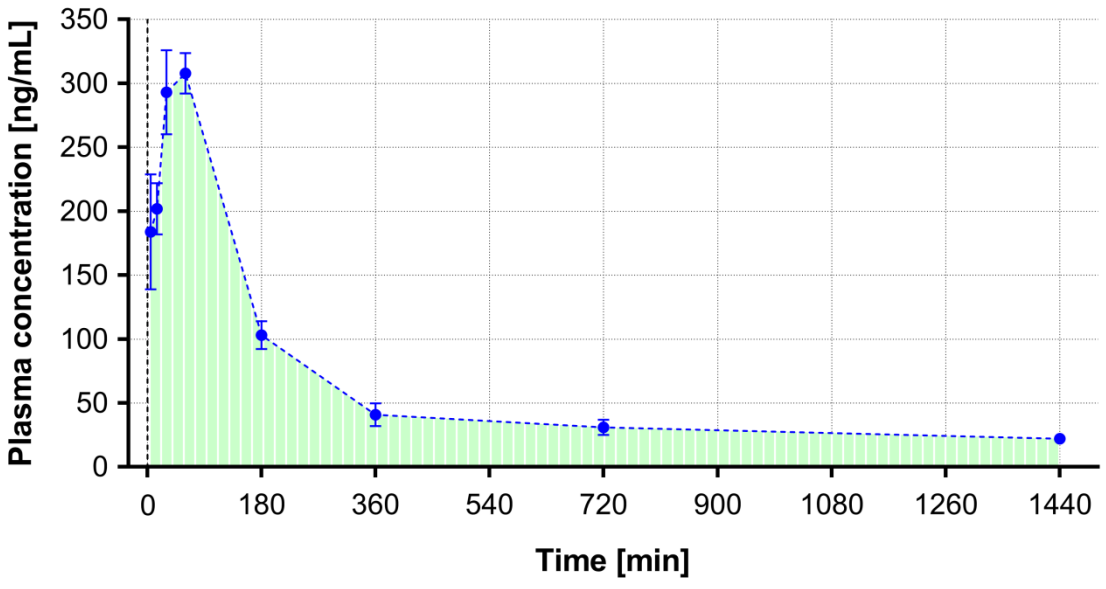

Fig. 8. Plasma concentration of compound **11** in mice (n = 6) after ip administration of 40 mg/kg.

2.9. Behavioral studies

The graphical representation of the applied protocols for behavioral studies of compound **11** has been depicted in Figure 9.

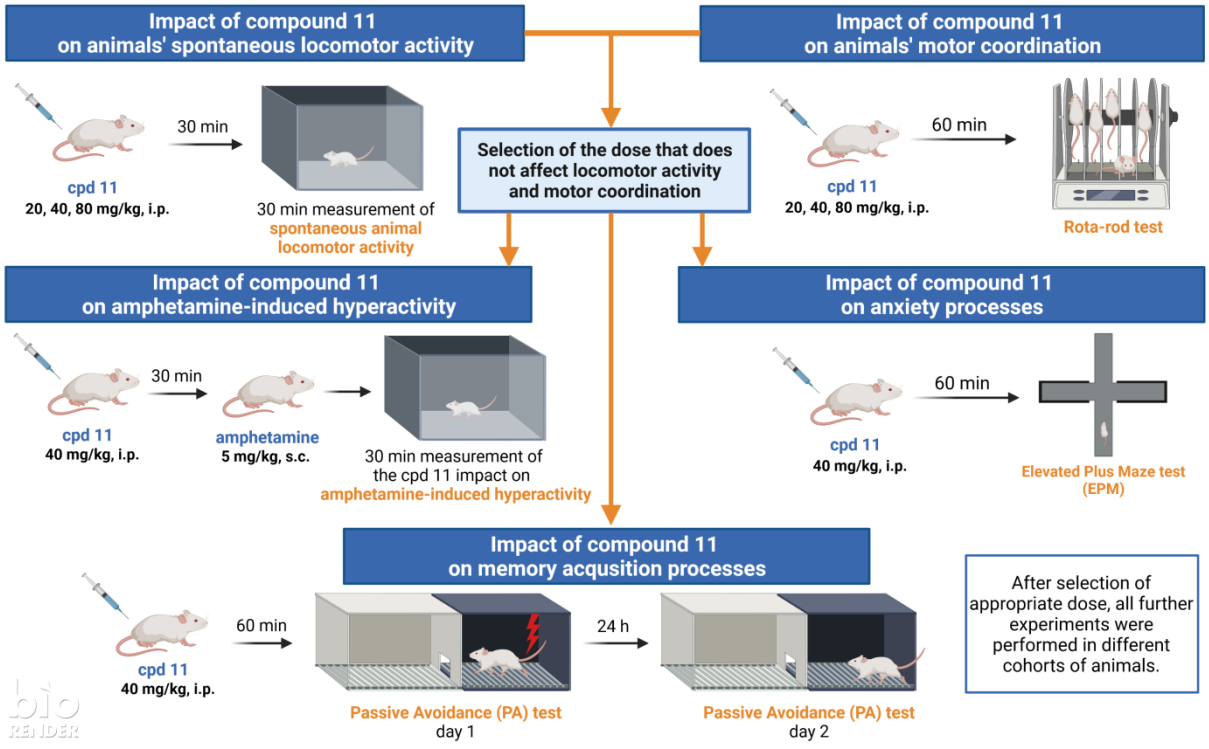

Fig. 9. Graphical summary of the applied behavioral protocol.

2.9.1. Compound 11 effects on motor coordination in mice

The studied compound **11** (20, 40, and 80 mg/kg) does not induce statistically significant changes in mouse motor coordination (one-way ANOVA: $F(3, 25) = 0.8263$, $p = 0.4919$). In particular, the ability of animals to keep balance on a rotating rod during 60 s (mean ± SEM) was measured for each dose of the studied compound (20 mg/kg: 60.00; 40 mg/kg: 55.50 ± 4.50; 80 mg/kg: 59.71 ± 0.28 and control group: 60.00).

2.9.2. Effects of compound 11 on spontaneous locomotor activity

As presented in Fig. 10, one-way ANOVA revealed that compound **11** (20, 40 and 80 mg/kg) induces statistically significant changes in spontaneous locomotor activity in mice [$F(3,23) = 3.673$, $p = 0.0262$]. Moreover, the Bonferroni's post hoc test revealed a statistically significant effect after 80 mg/kg compound **11** treatment compared to the vehicle-treated group ($p < 0.01$).

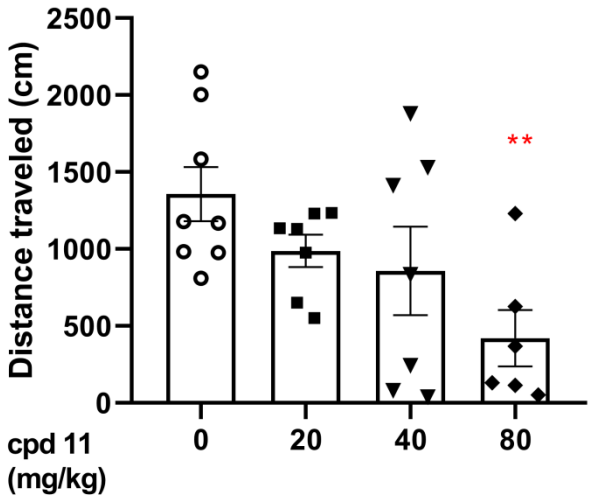

Fig. 10. Acute effects of compound **11** on mouse spontaneous locomotor activity. Compound **11** (20, 40 and 80 mg/kg, i.p., n = 7) or vehicle (n = 8) were injected and after 30 min the spontaneous locomotor activity was recorded for 30 min. The Bonferroni's post hoc test indicated the decrease in animal locomotor activity after the administration of compound **11** at the dose of 80 mg/kg: $^{**}p = 0.0094$.

2.9.3. Effects of compound 11 on amphetamine-induced hyperactivity in mice

To assess the influence of compound **11** on amphetamine-induced hyperactivity in mice the dose of 40 mg/kg was selected. Two-way ANOVA revealed that after co-administration of compound **11** (40 mg/kg, i.p.) with amphetamine (5 mg/kg, s.c.) there is a statistically significant pretreatment effect [$F(1, 27) = 41.58$, $p < 0.0001$], treatment effect [$F(1, 27) = 65.50$, $p < 0.0001$], and statistically significant interaction effect between treatment and

pretreatment [F (1, 27) = 36.27, $p < 0.0001$]. Moreover, the Bonferroni's post hoc test revealed that amphetamine treatment increased mice locomotor activity when compared to the control group (****$p < 0.0001$), and that amphetamine-induced hyperactivity is decreased by compound **11** administration ($^{\&\&\&\&}p < 0.0001$) as presented in Fig. 11.

The effect on amphetamine-induced hyperactivity is a classic test for evaluating the antipsychotic potential of new drug candidates [37]. An elevated locomotor activity is associated with an increase in mesolimbic dopamine concentration after amphetamine administration, therefore antagonizing this effect by lowering dopamine levels is considered an indicator of antipsychotic activity. Compound **11** is a dopamine D_2 receptor antagonist, as demonstrated in binding and functional studies, therefore it can be concluded that its effect on amphetamine-induced hyperactivity reduction, and thus antipsychotic activity, is mediated by its influence on this particular receptor.

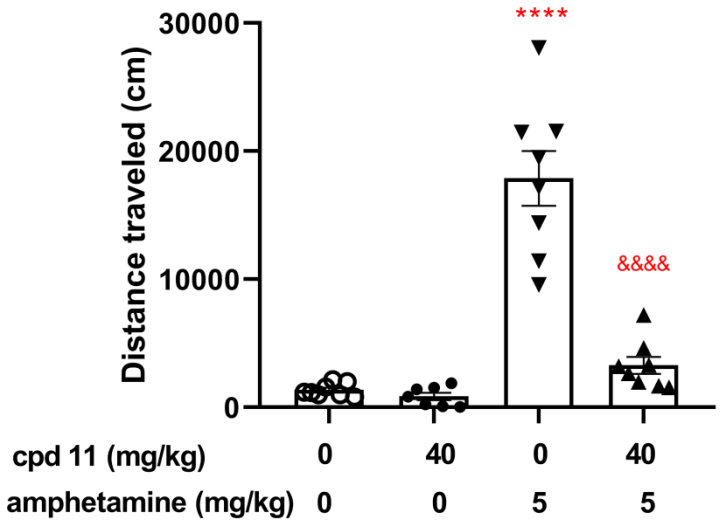

Fig. 11. Acute effect of compound **11** on amphetamine-induced hyperactivity in mice. Appropriate groups of mice received compound **11** [40 mg/kg; i.p. (n = 7)], amphetamine [5 mg/kg, s.c. (n = 8)], 40 mg/kg compound **11** co-injected with 5 mg/kg amphetamine (n = 8), and vehicle (n = 8) indicated as 0. Mice were injected with compound **11** or vehicle, and after

30 min received the second injection with vehicle or amphetamine. Immediately after the second injection animals' locomotion was recorded for 30 min. Data are presented as the distance traveled (cm) by animal (mean ± SEM). The results from the Bonferroni's post hoc test indicated: ****$p < 0.0001$ amphetamine vs. the vehicle-treated group and $^{\&\&\&\&}p < 0.0001$ for compound **11** co-administered with amphetamine vs. amphetamine-treated group.

2.9.4. Compound 11 effects on memory processes using passive avoidance (PA) test

As presented in Fig. 12, t-test ($p = 0.296$) revealed that 40 mg/kg compound **11** did not show an effect on the mouse memory acquisition process evaluated in the PA test. Memory impairment frequently occurs in schizophrenic patients and is one of the symptoms that is not effectively treated with the currently available antipsychotics. Moreover, some neuroleptics, such as clozapine, olanzapine, asenapine or lurasidone, may even exacerbate cognitive deficits, as they are shown to impair PA performance [38]. In this regard, the lack of effect of compound **11** on PA performance appears to be beneficial. It is suggested that the above effect is due to the antagonism of the serotonin 5-HT_{2A} receptor. It has been shown that the administration of agonists of this receptor improves memory processes, while the administration of an antagonist reverses this effect [39]. Compound D2AAK3, in contrast, shows an improvement in memory acquisition in the PA assay [17], which may be related to its approximately two-fold lower affinity for the 5-HT_{2A} receptor, compared to compound **11**.

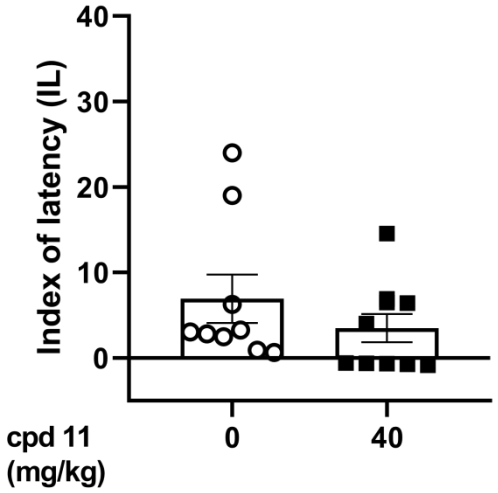

Fig. 12. Acute effect of compound **11** on memory acquisition in mice assessed in PA test. Appropriate groups of mice received acute injections with **11** [40 mg/kg, i.p. (n = 10)] and vehicle (n = 9) on Day 1 and, after 1h, were subjected to the PA test. Then, these rodents were retested on Day 2 (i.e., 24h later). Data are presented as the mean ± SEM of the latency index. T-test revealed the lack of statistically significant influence of compound **11** on memory acquisition in mice ($p = 0.296$).

2.9.5. Influence of compound 11 on anxiety-like behavior

T-test revealed that studied compound **11** (40 mg/kg) did not show an effect on anxiety-like behavior assessed after acute treatment in the elevated plus maze (EPM) test. More specifically, there is no influence on the percentage of the time spent in open arms ($p = 0.428$) (Fig. 13A) and the open arm entries ($p = 0.684$) (Fig. 13B). In addition, the number of entries to enclosed arms was calculated (Fig. 13C) and t-test indicated a lack of the difference between compound **11**-treated group and respective control group ($p = 0.173$). It is in agreement with spontaneous locomotor activity results presented in Fig. 10.

Anxiety processes can be regulated by affecting the serotonin 5-HT_{1A} receptor [40]. Preclinical and clinical data suggest that the direction of the effect on anxiety mediated by

agonists of the 5-HT_{1A} receptor depends on the location of this receptor. Activation of presynaptic autoreceptor populations in dorsal or median raphe nuclei leads to an anxiolytic effect, while activation of populations located postsynaptically in structures such as the amygdala or hippocampus produces an anxiogenic effect [41,42]. Compound **11** is a 5-HT_{1A} receptor agonist and shows no influence on anxiety in the EPM test, which may indicate that it has a comparable effect on presynaptic and postsynaptic 5-HT_{1A} receptors. Interestingly, despite a very similar affinity to the 5-HT_{1A} receptor as compound **11**, D2AAK3 showed an anxiogenic effect after 30 minutes after administration in the EPM test. This may be due to the different doses used and the difference in agonist potency between those compounds, as demonstrated in functional studies [17].

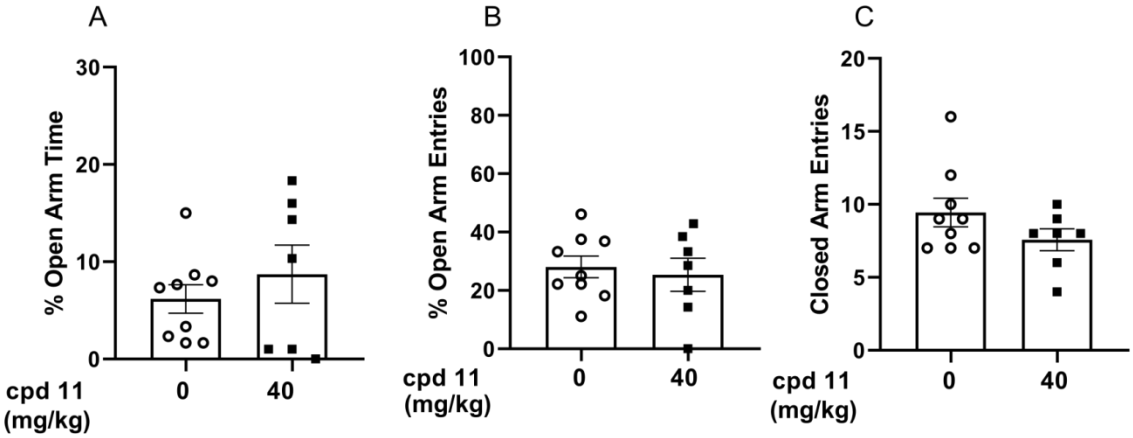

Fig. 13. Compound **11** (40 mg/kg, i.p.) effect on anxiety-like behavior using EPM performance in mice. Investigated compound **11** was injected i.p. 60 min before the test. The values represent the mean ± SEM of percentage of open arms time (A), percentage of entries into the open arms (B), and total arm entries counted as the sum of entries into open and enclosed arms (C). T-test: $p = 0.428$, $p = 0.684$, and $p = 0.173$ vs. control group for each presented group.

3. Conclusions

Schizophrenia is a disease of the central nervous system characterized by a complex etiology and still not fully understood underlying causes. Currently available antipsychotics are often ineffective, especially in relation to negative symptoms and cognitive deficits, therefore efforts should be made to develop new, more effective drugs. In this work, we focused on the development of novel multi-target molecules with a receptor profile similar to atypical antipsychotics. This approach is currently one of the most favored in the search for new antipsychotics, as it is believed that targeting several neurotransmitter systems simultaneously allows for better control of the disease and may also reduce the risk of adverse reactions.

The compound D2AAK3 identified in a virtual screening in our previous studies displays an affinity for dopamine and serotonin receptors, in particular for the D_2, 5-HT_{1A} and 5-HT_{2A} receptors, and also shows antipsychotic activity in behavioral assays, therefore it was selected for further development as a potential antipsychotic. As part of the optimization campaign, derivatives of D2AAK3 were designed and synthesized by introducing modifications to the arylpiperazine system and extending the linker connecting the distal fragments of the molecule. Then, the obtained compounds **1** – **17** were subjected to detailed structural and biological evaluation.

The affinities of the designed derivatives for the receptors of interest were determined and the compounds were analyzed for the structure-activity relationship. Derivatives with a more atypical receptor profile, i.e. a higher 5-HT_{2A}/D_2 affinity ratio than D2AAK3, were selected for functional assays, in which they were proven to be D_2 and 5-HT_{2A} antagonists and 5-HT_{1A} agonists. They also showed good selectivity over "off-targets", 5-HT_{2C}, H_1 and M_1 receptors. In order to study the interactions of compounds **1** – **17** with the above receptors at the molecular level, docking studies were performed, which revealed that the designed compounds adopt similar conformations in the binding pockets of the D_2 and 5-HT_{2A} receptors as D2AAK3, while in the case of the 5-HT_{1A} receptor, in contrast to D2AAK3, they are

positioned shallower in the binding pocket and rotated to form a "boat-like" shape. With the use of X-ray crystallography, the solid state conformation of compound **11**, selected for further evaluation, was also determined. ADMET assays carried out for compound **11** showed moderate potency to penetrate biological membranes, induction of CYP3A4, no neurotoxicity, and no interaction with P-glycoprotein. Plasma and brain concentrations of compound **11** at various time points were also measured, and the brain uptake was calculated. Behavioral tests for compound **11** confirmed its antipsychotic activity, as it decreased amphetamine-induced hyperactivity, but showed no effect on memory and anxiety processes in PA and EPM tests.

In summary, the research resulted in a series of D2AAK3 derivatives, some of which display an improved receptor profile and show beneficial effects in biological tests. However, in the further optimization process, issues such as improving ADMET parameters or obtaining molecules with better PA performance should be addressed.

4. Materials and methods

4.1. Chemistry

All reagents needed to carry out the synthesis were purchased from commercial vendors and were not subjected to further purification before use. NMR spectra were acquired on a Bruker AVANCE III 600 MHz or Bruker AVANCE III HD 500 MHz instrument with the use of DMSO-d6 or $CDCl_3$ as solvents. Chemical shifts are given in parts per million (δ), and are referenced to the residual proton signal in the respective solvent. Coupling constants (*J*) are reported in Hertz (Hz). High-resolution mass spectra (HRMS) were recorded on a Bruker microTOF-Q II mass spectrometer, with the application of electrospray ionization in the positive mode, with a time-of-flight (TOF) mass analyzer and the use of acetonitrile as solvent. Collected data were processed in MestReNova v.14.0.0 and Compass Data Analysis software. Analytical data for reported compounds are provided in Supplementary Information.

4.1.1. General procedure for the synthesis of compounds I – III

The appropriate aniline (25 mmol) and bis(2-chloroethyl)amine hydrochloride (25 mmol) were placed in a flask to which then 8 mL of diethylene glycol monomethyl ether was added. The mixture was stirred and heated at 150 °C for 16 hours. After this time, the mixture was cooled to ambient temperature and 25 mL of methanol was added. Then, 100 mL of ethyl acetate was added to the resulting solution, which led to the precipitation of the corresponding arylpiperazine hydrochloride. The resulting salt was washed with ethyl acetate and then converted to free amine by treatment with saturated sodium carbonate solution and extraction with ethyl acetate. The collected organic layers were dried over anhydrous magnesium sulfate and the solvent was evaporated to give the target piperazine.

4.1.2. Synthesis of compound 1a

A round bottom flask equipped with a reflux condenser was charged with phthalimide (0.2 mol), anhydrous potassium carbonate (0.2 mol), 1,4-dibromobutane (0.6 mol) and butan-2-one (250 mL). The mixture was stirred and refluxed for 10 hours, then cooled to room temperature. The inorganic salt precipitates were filtered off and washed with solvent. The combined filtrates were concentrated in a vacuum evaporator, and the resulting oily substance was crystallized from *n*-heptane.

4.1.3. General procedure for the synthesis of compounds 1b – 17b

2-(4-bromobutyl)isoindoline-1,3-dione (compound **1a**) (3 mmol), the corresponding *N*-substituted piperazine (3 mmol), anhydrous potassium carbonate (6 mmol) and a catalytic amount of potassium iodide were placed in a round bottom flask. Acetonitrile (9 mL) was then added and the reaction mixture was refluxed for 5-22 hours (TLC monitored). After cooling to ambient temperature, the solids were filtered off, washed with acetonitrile and the solvent was

evaporated under reduced pressure. The resulting product was used in the next step without further purification.

4.1.4. General procedure for the synthesis of compounds 1c – 17c

The appropriate intermediate obtained in the previous step was dissolved in ethanol 96%, then hydrazine monohydrate (1.3 eq.) was added and the mixture was stirred and refluxed for 3 hours. After cooling down water was added to dissolve the resulting precipitate, and the ethanol was distilled off. The resulting solution was adjusted to pH=1 with a solution of hydrochloric acid and the obtained precipitate was filtered off. The filtrate was adjusted to pH=10 with sodium hydroxide solution and then it was extracted three times with dichloromethane. The combined extracts were dried over anhydrous magnesium sulfate and the solvent was evaporated. The obtained product was used in the next step without purification.

4.1.5. General procedure for the synthesis of compounds 1 – 17

1*H*-indazole-3-carboxylic acid (1 mmol) and 1,1'-carbonyldiimidazole (CDI) (1 mmol) were dissolved in dimethylformamide (3 mL) and heated at 60°C for 2 hours. Then the appropriate primary amine (1 mmol) obtained in the previous step was dissolved in dimethylformamide (3 mL), added to the reaction mixture and heated at 60°C for 2.5 hours. After this time, the reaction mixture was concentrated and the residue dissolved in dichloromethane and washed sequentially with water, 1% sodium hydroxide solution and brine. The solution was dried over anhydrous magnesium sulfate, and then the solvent was evaporated. The resulting crude product was purified by washing with acetonitrile, or crystallization from acetonitrile, or by dry column vacuum chromatography (silica gel, MeOH/DCM, 2-6% gradient).

N-(4-(4-phenylpiperazin-1-yl)butyl)-1H-indazole-3-carboxamide (1)

Compound purified by DCVC (MeOH/DCM, 2-6% gradient): white solid. Overall yield: 31%. ^{1}H NMR (500 MHz, DMSO) δ 13.53 (s, 1H), 8.39 (t, *J* = 6.0 Hz, 1H), 8.21 – 8.15 (m, 1H), 7.63 – 7.57 (m, 1H), 7.44 – 7.37 (m, 1H), 7.26 – 7.16 (m, 3H), 6.94 – 6.87 (m, 2H), 6.79 – 6.72 (m, 1H), 3.33 – 3.30 (m, 2H), 3.13 – 3.07 (m, 4H), 2.50 – 2.47 (m, 4H), 2.34 (t, *J* = 7.2 Hz, 2H), 1.59 (dq, *J* = 11.3, 6.7 Hz, 2H), 1.55 – 1.47 (m, 2H). ^{13}C NMR (126 MHz, DMSO) δ 162.19, 151.07, 141.07, 138.45, 128.88, 126.42, 121.89, 121.64, 121.47, 118.69, 115.28, 110.61, 57.57, 52.77, 48.19, 38.25, 27.30, 23.84. HRMS (ESI) m/z $[M+H]^+$ calculated for $C_{22}H_{27}N_5O$: 378.2288, found: 378.2275.

N-(4-(4-(2-methoxyphenyl)piperazin-1-yl)butyl)-1H-indazole-3-carboxamide (2)

Compound purified by washing with ACN: white solid. Overall yield: 38%. ^{1}H NMR (600 MHz, DMSO) δ 13.27 (s, 1H), 8.40 (t, *J* = 5.9 Hz, 1H), 8.19 (dt, *J* = 8.2, 1.1 Hz, 1H), 7.61 (dt, *J* = 8.4, 1.0 Hz, 1H), 7.41 (ddd, *J* = 8.2, 6.8, 1.1 Hz, 1H), 7.24 (ddd, *J* = 8.0, 6.8, 0.9 Hz, 1H), 6.96 – 6.89 (m, 2H), 6.87 – 6.84 (m, 2H), 3.76 (s, 3H), 3.34 (q, *J* = 6.7 Hz, 2H), 2.94 (s, 4H), 2.55 – 2.41 (m, 4H), 2.35 (t, *J* = 7.2 Hz, 2H), 1.63 – 1.55 (m, 2H), 1.55 – 1.47 (m, 2H). ^{13}C NMR (151 MHz, DMSO) δ 162.70, 152.45, 141.80, 141.57, 138.95, 126.89, 122.75, 122.36, 122.12, 121.95, 121.31, 118.33, 112.39, 111.08, 58.12, 55.77, 53.52, 50.54, 38.76, 27.78, 24.32. HRMS (ESI) m/z $[M+H]^+$ calculated for $C_{23}H_{29}N_5O_2$: 408.2394, found: 408.2394.

N-(4-(4-(3-methoxyphenyl)piperazin-1-yl)butyl)-1H-indazole-3-carboxamide (3)

Compound purified by washing with ACN: white solid. Overall yield: 41%. ^{1}H NMR (600 MHz, DMSO) δ 13.50 (s, 1H), 8.41 (t, *J* = 6.0 Hz, 1H), 8.18 (d, *J* = 8.1 Hz, 1H), 7.61 (d, *J* = 8.4 Hz, 1H), 7.44 – 7.38 (m, 1H), 7.23 (t, *J* = 7.5 Hz, 1H), 7.09 (t, *J* = 8.2 Hz, 1H), 6.50 (dd, *J* = 8.3, 2.3 Hz, 1H), 6.42 (t, *J* = 2.4 Hz, 1H), 6.35 (dd, *J* = 8.1, 2.3 Hz, 1H), 3.70 (s, 3H), 3.33 (q, *J* = 6.7 Hz, 2H), 3.10 (t, *J* = 4.9 Hz, 4H), 2.48 (t, *J* = 5.0 Hz, 4H), 2.34 (t, *J* = 7.2 Hz, 2H), 1.59 (p, *J* = 6.9 Hz, 2H), 1.55 – 1.47 (m, 2H). ^{13}C NMR (151 MHz, DMSO) δ 162.68, 160.64,

152.91, 141.55, 138.93, 130.03, 126.90, 122.37, 122.10, 121.93, 111.09, 108.44, 104.50, 101.84, 58.03, 55.30, 53.22, 48.62, 38.72, 27.77, 24.31. HRMS (ESI) m/z $[M+H]^+$ calculated for $C_{23}H_{29}N_5O_2$: 408.2394, found: 408.2393.

N-(4-(4-(4-methoxyphenyl)piperazin-1-yl)butyl)-1H-indazole-3-carboxamide (4)

Compound purified by DCVC (MeOH/DCM, 2-6% gradient): white solid. Overall yield: 29%. ^{1}H NMR (500 MHz, $CDCl_3$) δ 10.58 (s, 1H), 8.40 (dt, *J* = 8.2, 1.0 Hz, 1H), 7.47 (dt, *J* = 8.5, 1.0 Hz, 1H), 7.44 – 7.39 (m, 1H), 7.30 – 7.26 (m, 2H), 6.92 – 6.87 (m, 2H), 6.86 – 6.81 (m, 2H), 3.76 (s, 3H), 3.54 (q, *J* = 6.5 Hz, 2H), 3.15 – 3.08 (m, 4H), 2.67 – 2.60 (m, 4H), 2.47 (t, *J* = 7.1 Hz, 2H), 1.76 – 1.62 (m, 4H). ^{13}C NMR (126 MHz, $CDCl_3$) δ 162.78, 153.80, 145.73, 141.30, 139.66, 127.32, 122.78, 122.76, 122.00, 118.18, 114.45, 109.67, 58.12, 55.59, 53.37, 50.54, 38.92, 27.72, 24.37. HRMS (ESI) m/z $[M+H]^+$ calculated for $C_{23}H_{29}N_5O_2$: 408.2394, found: 408.2393.

N-(4-(4-(pyridin-2-yl)piperazin-1-yl)butyl)-1H-indazole-3-carboxamide (5)

Compound purified by washing with ACN: white solid. Overall yield: 29%. ^{1}H NMR (600 MHz, DMSO) δ 13.53 (s, 1H), 8.40 (t, *J* = 5.9 Hz, 1H), 8.19 (d, *J* = 8.1 Hz, 1H), 8.09 (dd, *J* = 5.0, 2.0 Hz, 1H), 7.61 (d, *J* = 8.4 Hz, 1H), 7.50 (ddd, *J* = 8.8, 7.0, 2.0 Hz, 1H), 7.44 – 7.38 (m, 1H), 7.24 (t, *J* = 7.5 Hz, 1H), 6.78 (d, *J* = 8.6 Hz, 1H), 6.62 (dd, *J* = 7.1, 4.8 Hz, 1H), 3.47 – 3.42 (m, 4H), 3.34 (q, *J* = 6.6 Hz, 2H), 2.43 (t, *J* = 5.0 Hz, 4H), 2.33 (t, *J* = 7.2 Hz, 2H), 1.63 – 1.55 (m, 2H), 1.55 – 1.48 (m, 2H). ^{13}C NMR (151 MHz, DMSO) δ 162.70, 159.56, 148.00, 141.57, 138.95, 137.90, 126.90, 122.37, 122.11, 121.95, 113.36, 111.08, 107.46, 58.10, 53.06, 45.13, 38.73, 27.78, 24.29. HRMS (ESI) m/z $[M+H]^+$ calculated for $C_{21}H_{26}N_6O$: 379.2241, found: 379.2241.

N-(4-(4-(pyridin-3-yl)piperazin-1-yl)butyl)-1H-indazole-3-carboxamide (6)

Compound purified by washing with ACN: white solid. Overall yield: 16%. ^{1}H NMR (600 MHz, DMSO) δ 13.54 (s, 1H), 8.40 (t, *J* = 5.9 Hz, 1H), 8.28 (d, *J* = 3.0 Hz, 1H), 8.19 (d, *J* = 8.1 Hz, 1H), 8.00 – 7.96 (m, 1H), 7.61 (d, *J* = 8.4 Hz, 1H), 7.44 – 7.38 (m, 1H), 7.31 – 7.26 (m, 1H), 7.24 (t, *J* = 7.5 Hz, 1H), 7.19 (dd, *J* = 8.5, 4.5 Hz, 1H), 3.34 (q, *J* = 6.6 Hz, 2H), 3.17 (t, *J* = 5.0 Hz, 4H), 2.50 – 2.47 (m, 4H), 2.35 (t, *J* = 7.2 Hz, 2H), 1.59 (p, *J* = 6.9 Hz, 2H), 1.55 – 1.48 (m, 2H). ^{13}C NMR (151 MHz, DMSO) δ 162.70, 147.16, 141.57, 140.02, 138.95, 138.02, 126.90, 123.93, 122.37, 122.11, 122.05, 121.95, 111.08, 57.98, 52.96, 47.98, 38.73, 27.75, 24.27. HRMS (ESI) m/z $[M+H]^+$ calculated for $C_{21}H_{26}N_6O$: 379.2241, found: 379.2241.

N-(4-(4-(pyridin-4-yl)piperazin-1-yl)butyl)-1H-indazole-3-carboxamide (7)

Compound purified by washing with ACN: white solid. Overall yield: 13%. ^{1}H NMR (600 MHz, DMSO) δ 13.55 (s, 1H), 8.41 (t, *J* = 6.0 Hz, 1H), 8.18 (d, *J* = 8.2 Hz, 1H), 8.14 (d, *J* = 5.7 Hz, 2H), 7.61 (d, *J* = 8.4 Hz, 1H), 7.41 (t, *J* = 7.6 Hz, 1H), 7.24 (t, *J* = 7.5 Hz, 1H), 6.81 – 6.76 (m, 2H), 3.33 (q, *J* = 6.7 Hz, 2H), 3.28 (t, *J* = 5.1 Hz, 4H), 2.45 (t, *J* = 5.1 Hz, 4H), 2.34 (t, *J* = 7.2 Hz, 2H), 1.59 (p, *J* = 6.9 Hz, 2H), 1.51 (p, *J* = 7.0, 6.6 Hz, 2H). ^{13}C NMR (151 MHz, DMSO) δ 162.70, 155.01, 150.25, 141.56, 138.93, 126.91, 122.39, 122.10, 121.94, 111.09, 108.76, 57.93, 52.74, 45.88, 38.71, 27.73, 24.23. HRMS (ESI) m/z $[M+H]^+$ calculated for $C_{21}H_{26}N_6O$: 379.2241, found: 379.2241.

N-(4-(4-(pyrimidin-2-yl)piperazin-1-yl)butyl)-1H-indazole-3-carboxamide (8)

Compound purified by DCVC (MeOH/DCM, 2-6% gradient): white solid. Overall yield: 27%. ^{1}H NMR (500 MHz, $CDCl_3$) δ 11.46 (s, 1H), 8.39 (dt, *J* = 8.2, 1.1 Hz, 1H), 8.30 (d, *J* = 4.8 Hz, 2H), 7.47 (dt, *J* = 8.4, 0.9 Hz, 1H), 7.40 – 7.36 (m, 1H), 7.34 (t, *J* = 6.0 Hz, 1H), 7.27 – 7.23 (m, 1H), 6.48 (t, *J* = 4.7 Hz, 1H), 3.88 – 3.83 (m, 4H), 3.54 (q, *J* = 6.4 Hz, 2H), 2.54 – 2.49 (m, 4H), 2.46 – 2.40 (m, 2H), 1.75 – 1.60 (m, 4H). ^{13}C NMR (126 MHz, $CDCl_3$) δ 162.99, 161.62, 157.71, 141.39, 139.39, 127.15, 122.66, 122.62, 121.99, 109.86, 109.80, 58.10, 53.07, 43.59,

38.89, 27.59, 24.27. HRMS (ESI) m/z $[M+H]^+$ calculated for $C_{20}H_{25}N_7O$: 380.2193, found: 380.2193.

N-(4-(4-(2-fluorophenyl)piperazin-1-yl)butyl)-1H-indazole-3-carboxamide (9)

Compound purified by washing with ACN: white solid. Overall yield: 35%. ^{1}H NMR (600 MHz, DMSO) δ 13.55 (s, 1H), 8.42 (t, *J* = 5.9 Hz, 1H), 8.19 (d, *J* = 8.1 Hz, 1H), 7.61 (d, *J* = 8.4 Hz, 1H), 7.44 – 7.38 (m, 1H), 7.27 – 7.21 (m, 1H), 7.14 – 7.06 (m, 2H), 7.03 – 6.98 (m, 1H), 6.98 – 6.92 (m, 1H), 3.34 (q, *J* = 6.7 Hz, 2H), 3.03 – 2.96 (m, 4H), 2.55 – 2.51 (m, 4H), 2.36 (t, *J* = 7.2 Hz, 2H), 1.64 – 1.55 (m, 2H), 1.55 – 1.47 (m, 2H). ^{13}C NMR (151 MHz, DMSO) δ 162.69, 155.41 (d, *J* = 244.2 Hz), 141.56, 140.39 (d, *J* = 8.3 Hz), 138.94, 126.90, 125.25 (d, *J* = 3.3 Hz), 122.62 (d, *J* = 8.0 Hz), 122.37, 122.12, 121.95, 119.57 (d, *J* = 3.0 Hz), 116.34 (d, *J* = 20.6 Hz), 111.08, 57.99, 53.26, 50.58 (d, *J* = 3.2 Hz), 38.73, 27.74, 24.29. HRMS (ESI) m/z $[M+H]^+$ calculated for $C_{22}H_{26}FN_5O$: 396.2194, found: 396.2194.

N-(4-(4-(3-fluorophenyl)piperazin-1-yl)butyl)-1H-indazole-3-carboxamide (10)

Compound purified by washing with ACN: white solid. Overall yield: 45%. ^{1}H NMR (600 MHz, DMSO) δ 13.54 (s, 1H), 8.41 (t, *J* = 6.0 Hz, 1H), 8.18 (d, *J* = 8.2 Hz, 1H), 7.61 (d, *J* = 8.4 Hz, 1H), 7.41 (dd, *J* = 8.3, 7.0 Hz, 1H), 7.26 – 7.16 (m, 2H), 6.76 – 6.68 (m, 2H), 6.53 (td, *J* = 8.3, 2.4 Hz, 1H), 3.33 (q, *J* = 6.6 Hz, 2H), 3.15 (t, *J* = 5.0 Hz, 4H), 2.48 (d, *J* = 5.1 Hz, 4H), 2.35 (p, *J* = 7.6, 6.9 Hz, 2H), 1.59 (p, *J* = 6.9 Hz, 2H), 1.52 (ddd, *J* = 14.6, 8.5, 5.9 Hz, 2H). ^{13}C NMR (151 MHz, DMSO) δ 163.75 (d, *J* = 240.2 Hz), 162.77, 153.31 (d, *J* = 10.0 Hz), 141.87, 138.88, 130.72 (d, *J* = 10.1 Hz), 126.69, 122.25, 122.06, 122.01, 111.24, 111.21 (d, *J* = 2.0 Hz), 104.97 (d, *J* = 21.3 Hz), 102.07 (d, *J* = 25.2 Hz), 57.97, 53.02, 48.13, 38.71, 27.78, 24.30. HRMS (ESI) m/z $[M+H]^+$ calculated for $C_{22}H_{26}FN_5O$: 396.2194, found: 396.2192.

N-(4-(4-(4-fluorophenyl)piperazin-1-yl)butyl)-1H-indazole-3-carboxamide (11)

Compound purified by crystallization from ACN: white solid. Overall yield: 27%. ^{1}H NMR (600 MHz, DMSO) δ 13.56 (s, 1H), 8.41 (t, *J* = 6.0 Hz, 1H), 8.21 – 8.18 (m, 1H), 7.64 – 7.60 (m, 1H), 7.41 (ddd, *J* = 8.2, 6.8, 1.1 Hz, 1H), 7.24 (ddd, *J* = 7.9, 6.8, 0.9 Hz, 1H), 7.06 – 7.00 (m, 2H), 6.94 – 6.89 (m, 2H), 3.33 (q, *J* = 6.7 Hz, 2H), 3.08 – 3.02 (m, 4H), 2.50 – 2.47 (m, 4H), 2.34 (t, *J* = 7.2 Hz, 2H), 1.59 (p, *J* = 6.9 Hz, 2H), 1.51 (p, *J* = 7.0, 6.5 Hz, 2H). ^{13}C NMR (151 MHz, DMSO) δ 162.70, 156.39 (d, *J* = 235.4 Hz), 148.44 (d, *J* = 1.9 Hz), 141.57, 138.92, 126.89, 122.37, 122.11, 121.94, 117.45 (d, *J* = 7.6 Hz), 115.67 (d, *J* = 21.8 Hz), 111.11, 57.99, 53.20, 49.44, 38.73, 27.77, 24.30. HRMS (ESI) m/z $[M+H]^+$ calculated for $C_{22}H_{26}FN_5O$: 396.2194, found: 396.2195.

N-(4-(4-(2-(trifluoromethyl)phenyl)piperazin-1-yl)butyl)-1H-indazole-3-carboxamide (12)

Compound purified by washing with ACN: white solid. Overall yield: 45%. ^{1}H NMR (600 MHz, DMSO) δ 13.55 (s, 1H), 8.42 (t, *J* = 6.0 Hz, 1H), 8.20 – 8.17 (m, 1H), 7.67 – 7.59 (m, 3H), 7.52 (d, *J* = 8.0 Hz, 1H), 7.43 – 7.39 (m, 1H), 7.31 (t, *J* = 7.6 Hz, 1H), 7.25 – 7.22 (m, 1H), 3.33 (q, *J* = 6.7 Hz, 2H), 2.88 – 2.84 (m, 4H), 2.60 – 2.51 (m, 4H), 2.38 (t, *J* = 7.2 Hz, 2H), 1.59 (p, *J* = 6.9 Hz, 2H), 1.51 (p, *J* = 7.1, 6.6 Hz, 2H). ^{13}C NMR (151 MHz, DMSO) δ 162.71, 152.87 (q, *J* = 1.5 Hz), 141.56, 138.94, 134.01, 127.37 (q, *J* = 5.4 Hz), 126.90, 126.01 (q, *J* = 28.0 Hz), 125.50, 124.83, 124.58 (q, *J* = 273.2 Hz), 122.37, 122.10, 121.94, 111.08, 57.96, 53.56, 53.53, 38.71, 27.73, 24.21. HRMS (ESI) m/z $[M+H]^+$ calculated for $C_{23}H_{26}F_3N_5O$: 446.2162, found: 446.2162.

N-(4-(4-(3-(trifluoromethyl)phenyl)piperazin-1-yl)butyl)-1H-indazole-3-carboxamide (13)

Compound purified by washing with ACN: white solid. Overall yield: 27%. ^{1}H NMR (600 MHz, DMSO) δ 13.55 (s, 1H), 8.41 (t, *J* = 5.9 Hz, 1H), 8.19 (d, *J* = 8.1 Hz, 1H), 7.61 (d, *J* = 8.4 Hz, 1H), 7.44 – 7.37 (m, 2H), 7.23 (t, *J* = 7.5 Hz, 1H), 7.20 (dd, *J* = 8.4, 2.5 Hz, 1H), 7.15 – 7.13 (m, 1H), 7.05 (d, *J* = 7.6 Hz, 1H), 3.34 (q, *J* = 6.7 Hz, 2H), 3.22 – 3.18 (m, 4H), 2.50 –

2.47 (m, 4H), 2.35 (t, *J* = 7.2 Hz, 2H), 1.59 (p, *J* = 6.8 Hz, 2H), 1.52 (p, *J* = 7.1, 6.5 Hz, 2H). ^{13}C NMR (151 MHz, DMSO) δ 162.72, 151.61, 141.56, 138.93, 130.42, 130.33 (q, *J* = 30.9 Hz), 126.90, 124.91 (q, *J* = 272.5 Hz), 122.38, 122.10, 121.94, 119.12 (q, *J* = 1.3 Hz), 115.02 (q, *J* = 4.0, 3.6 Hz), 111.26 (q, *J* = 3.9 Hz), 111.09, 57.81, 52.87, 47.88, 38.68, 27.71, 24.08. HRMS (ESI) m/z $[M+H]^+$ calculated for $C_{23}H_{26}F_3N_5O$: 446.2162, found: 446.2163.

N-(4-(4-(2-chlorophenyl)piperazin-1-yl)butyl)-1H-indazole-3-carboxamide (14)

Compound purified by washing with ACN: white solid. Overall yield: 28%. ^{1}H NMR (600 MHz, DMSO) δ 13.51 (s, 1H), 8.40 (t, *J* = 5.9 Hz, 1H), 8.20 – 8.16 (m, 1H), 7.61 (d, *J* = 8.5 Hz, 1H), 7.43 – 7.37 (m, 2H), 7.28 (td, *J* = 7.7, 1.5 Hz, 1H), 7.25 – 7.22 (m, 1H), 7.13 (dd, *J* = 8.1, 1.5 Hz, 1H), 7.02 (td, *J* = 7.6, 1.5 Hz, 1H), 3.33 (d, *J* = 6.5 Hz, 2H), 2.97 (s, 4H), 2.59 – 2.51 (m, 4H), 2.37 (t, *J* = 7.2 Hz, 2H), 1.60 (p, *J* = 7.0 Hz, 2H), 1.52 (p, *J* = 7.1, 6.6 Hz, 2H). ^{13}C NMR (151 MHz, DMSO) δ 162.69, 149.55, 141.57, 138.94, 130.77, 128.51, 128.05, 126.90, 124.24, 122.37, 122.10, 121.94, 121.25, 111.09, 57.99, 53.36, 51.33, 38.73, 27.74, 24.30. HRMS (ESI) m/z $[M+H]^+$ calculated for $C_{22}H_{26}ClN_5O$: 412.1899, found: 412.1897.

N-(4-(4-(2-(methylthio)phenyl)piperazin-1-yl)butyl)-1H-indazole-3-carboxamide (15)

Compound was pure after workup – no additional purification needed: white solid. Overall yield: 49%. ^{1}H NMR (600 MHz, DMSO) δ 13.55 (s, 1H), 8.42 (t, *J* = 5.9 Hz, 1H), 8.21 – 8.16 (m, 1H), 7.63 – 7.59 (m, 1H), 7.43 – 7.39 (m, 1H), 7.26 – 7.21 (m, 1H), 7.14 – 7.03 (m, 4H), 3.33 (q, *J* = 6.7 Hz, 2H), 2.88 (s, 4H), 2.60 – 2.51 (m, 4H), 2.38 – 2.34 (m, 5H), 1.59 (p, *J* = 7.0 Hz, 2H), 1.51 (p, *J* = 7.0, 6.5 Hz, 2H). ^{13}C NMR (151 MHz, DMSO) δ 162.69, 149.65, 141.56, 138.94, 134.90, 126.90, 125.21, 124.68, 124.63, 122.38, 122.11, 121.94, 119.90, 111.09, 58.08, 53.60, 51.64, 38.74, 27.77, 24.32, 14.03. HRMS (ESI) m/z $[M+H]^+$ calculated for $C_{23}H_{29}N_5OS$: 424.2166, found: 424.2166.

N-(4-(4-(2-ethoxyphenyl)piperazin-1-yl)butyl)-1H-indazole-3-carboxamide (16)

Compound purified by washing with ACN: white solid. Overall yield: 37%. ^{1}H NMR (600 MHz, DMSO) δ 13.55 (s, 1H), 8.43 (t, *J* = 5.9 Hz, 1H), 8.18 (d, *J* = 8.1 Hz, 1H), 7.61 (d, *J* = 8.4 Hz, 1H), 7.41 (t, *J* = 7.6 Hz, 1H), 7.24 (t, *J* = 7.5 Hz, 1H), 6.93 – 6.82 (m, 4H), 3.99 (q, *J* = 6.9 Hz, 2H), 3.33 (q, *J* = 6.7 Hz, 2H), 2.97 (s, 4H), 2.49 (s, 4H), 2.35 (t, *J* = 7.2 Hz, 2H), 1.59 (p, *J* = 6.9 Hz, 2H), 1.52 (q, *J* = 7.8 Hz, 2H), 1.32 (t, *J* = 6.9 Hz, 3H). ^{13}C NMR (151 MHz, DMSO) δ 162.68, 151.59, 141.99, 141.55, 138.92, 126.90, 122.60, 122.37, 122.11, 121.94, 121.39, 118.31, 113.68, 111.09, 63.72, 58.13, 53.53, 50.46, 38.74, 27.78, 24.32, 15.31. HRMS (ESI) m/z $[M+H]^+$ calculated for $C_{24}H_{31}N_5O_2$: 422.2551, found: 422.2554.

N-(4-(4-cyclohexylpiperazin-1-yl)butyl)-1H-indazole-3-carboxamide (17)

Compound purified by washing with ACN: white solid. Overall yield: 29%. ^{1}H NMR (600 MHz, DMSO) δ 13.53 (s, 1H), 8.38 (t, *J* = 5.9 Hz, 1H), 8.17 (d, *J* = 8.1 Hz, 1H), 7.60 (d, *J* = 8.4 Hz, 1H), 7.40 (t, *J* = 7.6 Hz, 1H), 7.23 (t, *J* = 7.5 Hz, 1H), 3.30 (q, *J* = 6.7 Hz, 2H), 2.49 – 2.09 (m, 11H), 1.70 (t, *J* = 12.4 Hz, 4H), 1.54 (p, *J* = 6.8 Hz, 3H), 1.45 (p, *J* = 7.3 Hz, 2H), 1.23 – 0.99 (m, 5H). ^{13}C NMR (151 MHz, DMSO) δ 162.66, 141.55, 138.93, 126.87, 122.34, 122.11, 121.94, 111.06, 62.97, 58.16, 53.87, 48.86, 38.74, 28.85, 27.79, 26.40, 25.74, 24.36. HRMS (ESI) m/z $[M+H]^+$ calculated for $C_{22}H_{33}N_5O$: 384.2758, found: 384.2758.

4.2. Receptor radioligand binding assays

Competition radioligand binding assays were performed on in-house available membranes from cell lines exhibiting stable expression of the human cloned receptors. CHO-K1 cell lines stably expressing cloned human dopamine D_{2S} [43], serotonin 5-HT_{2A} [44], histamine H_1 [45] and muscarinic M_1 receptors, as well as a HEK293 cell line stably expressing the cloned human 5-HT_{1A} receptor [46], and a HeLa cell line stably expressing the cloned human 5-HT_{2C} receptor [47], were employed. Studied compounds were evaluated either at a single concentration of 10 μM or in competition binding curves, which were typically

constructed based on six different concentrations of a certain compound. The following reference compounds as internal controls were included in the assays: haloperidol (D_2), 5-carboxamidotryptamine (5-CT) (5-HT_{1A}), risperidone (5-HT_{2A} and 5-HT_{2C}), doxepin (H_1) and ipratropium (M_1). Assays (250 µL assay final volume) were carried out in 96-well polypropylene plates in duplicate. In brief, appropriate membrane protein suspension was incubated in assay buffer with added corresponding radioligand in presence or absence of test compound or reference compound. [^{3}H]-Spiperone (0.6 nM; D_2 receptor), [^{3}H]-8-OH-DPAT (1 nM; 5-HT_{1A} receptor), [^{3}H]-Ketanserin (1.25 nM; 5-HT_{2A}), [^{3}H]-Mesulergine (1.25 nM; 5-HT_{2C}), [^{3}H]-Pyrilamine (4 nM; H_1 receptor), and [^{3}H]-Pirenzepine (7 nM; M_1 receptor) were used as radioligands. In order to assess non-specific binding, membrane protein and radioligand were incubated in the presence of 100 µM sulpiride (D_2), 10 µM serotonin (5-HT_{1A}), 1 µM methysergide (5-HT_{2A}), 10 µM mianserin (5-HT_{2C}), 10 µM triprolidine (H_1), and 200 µM pirenzepine (M_1). After incubation, the content of the assay plates was transferred to glass fiber filter GF/B or GF/C 96 well plates pretreated with polyethyleneimine (PEI) and rapidly filtered using a vacuum manifold, followed by rapid washing with cold (4 °C) wash buffer. Then the filter plates were dried at 60 °C for 1h. After drying, 30 µL of liquid scintillation cocktail (UniverSol-ES, MP Biomedicals, Ohio, US) was added to each well of the plates and radioactivity was measured in a MicroBeta^2 microplate scintillation counter (PerkinElmer, Madrid, Spain). A detailed description of experimental conditions applied in radioligand binding assays for each receptor can be found in Supplementary Information (Table S3).

4.2.1. Radioligand binding data analysis

Competition binding curves were fitted to a one-site competition binding model (Fit Ki) using Prism 7 software (GraphPad, San Diego, CA). logK_i (log of the equilibrium dissociation constant (K_i) values were obtained after constraining the concentration of radioligand employed

in the assay and its dissociation constant (K_D) as determined in saturation radioligand binding assays.

4.3. Receptor functional assays

4.3.1. Functional assays of cAMP signaling at D_2 receptors

The activity of selected compounds at D_2 and 5-HT_{1A} receptors was investigated in cell-based functional assays of cAMP signaling, in the CHO-K1 cell line stably expressing the cloned human D_{2S} receptor also employed for the radioligand binding assays. For antagonism at D_2 receptors, test compounds were dispensed into an empty 96-well plate (Isoplate-96 Black Frame White Well, PerkinElmer España SL, Madrid, Spain) using an acoustic dispensing noncontact Echo 550 acoustic liquid handler (LABCYTE Inc., San Jose, CA, USA). Compounds were handled from frozen 10^{-2} M stock solutions in 100% DMSO, from which serial 1000x solutions were prepared in 100% DMSO at the time of the assay, keeping vehicle concentration (0.1% DMSO) constant in the assay. Vials of viable frozen cells were quickly thawed in a 37°C water bath and cells were seeded into the assay plate in assay buffer (kit stimulation buffer containing 500 µM 3-isobutyl-1-methylxanthine (IBMX) that was directly added to the buffer as powder). After 5 min incubation at 37°C, reference agonist dopamine (Dopamine hydrochloride, Sigma-Aldrich, Merck Life Science S.L.U., Madrid, Spain) (10^{-6} M final concentration, prepared from freshly made aqueous stock solution) was added to the corresponding wells. After 10 min incubation at 37°C, 10 µM forskolin was added to the corresponding wells and incubation was continued for 5 min. After this time, cellular cAMP levels were quantified using the homogeneous time-resolved fluorescence (HTRF)-based cAMP Gs dynamic kit (Cisbio, Bioassays, Codolet, France) according to the manufacturer's protocol. Haloperidol (10^{-10} - 10^{-5} M) was used as control antagonist in these assays. Basal cAMP levels were determined in control wells in the absence of compound, agonist, and forskolin. Concentration (10^{-10} M - 10^{-4} M) -response curves of dopamine were included in the

individual experiments for internal EC_{50} calculation. Individual concentration-response curves were fitted to the model of log(inhibitor) vs. response (three parameters) (Hill slope (n_H) = 1; best fit in comparison to log(inhibitor) vs. response -- Variable slope (four parameters) model, $P < 0.05$, extra sum-of-squares F test) described by the equation Y=Bottom + (Top-Bottom)/(1+10^((X-LogIC50))) using Prism 7 software (GraphPad, San Diego, CA) and pIC_{50} ($-logIC_{50}$) values were extracted from the fitting. K_b (equilibrium dissociation constant of a competitive antagonist determined by means of a functional assay) of the compounds was estimated according to the Leff-Dougall variant of the Cheng-Prusoff equation $K_b = IC_{50}/((2 + ([Ag]/[EC_{50}])^n)^{1/n} - 1)$, where IC_{50} is the concentration of antagonist that inhibits agonist response by a 50%; [Ag] is the concentration of agonist employed in the assay, $[EC_{50}]$ is the agonist EC_{50} value in the assay and n is the Hill slope of the concentration-response curve of the agonist [48].

4.3.2. Functional assays of cAMP signaling at 5-HT_{1A} receptors

The activity of selected compounds at 5-HT_{1A} receptors was investigated in cell-based functional assays of cAMP signaling in the HEK293 cell line stably expressing the cloned human 5-HT_{1A} receptor also employed for the radioligand binding assays. 24 hours before the experiment, cells in culture were seeded in complete growth medium prepared with dialyzed fetal bovine serum, in 96-well tissue culture plates (Greiner CELLSTAR® white 96 well plates, Sigma-Aldrich, Merck Life Science S.L.U., Madrid, Spain). On the day of assay, plates were washed with assay buffer (kit stimulation buffer containing 500 µM IBMX) and incubated with test compounds or control agonist 5-carboxamidotryptamine (10^{-12} M - 10^{-5} M) (5-Carboxamidotryptamine maleate salt, Sigma-Aldrich, Merck Life Science S.L.U., Madrid, Spain) for 10 min at 37°C. Test compounds were added to the assay plates from 5x working dilution intermediate plates that were prepared by means of acoustic noncontact dispensing of the compounds, keeping vehicle concentration (0.1% DMSO) constant in the assay. After this

time, 1 µM forskolin was added to the corresponding wells and incubation was continued for 5 min before cellular cAMP levels were quantified as described above for functional assays of cAMP signaling at D_2 receptors. Individual concentration-response curves were fitted to the model of log(agonist) vs. response (three parameters) (Hill slope (n_H) = 1; best fit in comparison to log(agonist) vs. response -- Variable slope (four parameters) model, $P < 0.05$, extra sum-of-squares F test) described by the equation Y=Bottom + (Top-Bottom)/(1+10^((LogEC50-X))) using Prism 7 software (GraphPad, San Diego, CA) and pEC_{50} ($-logEC_{50}$) values were extracted from the fitting.

4.3.3. Functional assays of inositol phosphate production at 5-HT_{2A} receptors

The activity of selected compounds at 5-HT_{2A} receptors was investigated in cell-based functional assays of inositol phosphate (IP) production in the CHO-K1 cell line stably expressing the cloned human 5-HT_{2A} receptor also employed for the radioligand binding assays. 24 hours before the experiment, cells in culture were seeded in complete growth medium prepared with dialyzed fetal bovine serum, in half-area, white, 96-well tissue culture plates (Corning®, Fisher Scientific SL, Madrid, Spain). On the day of assay, plates were washed with assay buffer (kit stimulation buffer) and incubated with test compounds for 10 min at 37°C. Test compounds were added to the assay plates from 7x working dilution intermediate plates that were prepared by means of acoustic noncontact dispensing of the compounds, keeping vehicle concentration (0.1% DMSO) constant in the assay. After this time, reference agonist serotonin (Serotonin hydrochloride, Sigma-Aldrich, Merck Life Science S.L.U., Madrid, Spain) (10^{-6} M final concentration, prepared from freshly made aqueous stock solution) was added to the corresponding wells and incubation was continued for 20 min at 37°C. After this time, cellular IP levels were quantified by using the homogeneous time-resolved fluorescence (HTRF)-based inositol monophosphate kit IP-One Gq kit (Cisbio, Bioassays, Codolet, France) following the manufacturer's protocol. Risperidone (10^{-12} - 10^{-7} M) was used as control

antagonist in these assays. Basal IP levels were determined in control wells in the absence of compound and agonist. Concentration (10^{-10} M - 10^{-4} M) -response curves of serotonin were included in the individual experiments for internal EC_{50} calculation. Individual concentration-response curves were fitted to the model of log(inhibitor) vs. response (three parameters) (Hill slope (n_H) = 1; best fit in comparison to log(inhibitor) vs. response -- Variable slope (four parameters) model, $P < 0.05$, extra sum-of-squares F test) described by the equation Y=Bottom + (Top-Bottom)/(1+10^((X-LogIC50))) using Prism 7 software (GraphPad, San Diego, CA) and pIC_{50} ($-logIC_{50}$) values were extracted from the fitting. K_b value of the compounds was estimated as described above for functional assays of cAMP signaling at D_2 receptors.

4.4. Molecular modeling

The modeling of ligands was performed using LigPrep protocol within Schrödinger software, version 2021-4 [49]. Epik module [50,51] of the same suite of software was applied to obtain the protonated states of the compounds. The following X-ray structures were used for docking studies: inactive conformation of dopamine D_2 receptor in complex with antagonist risperidone (PDB ID: 6CM4) [52], active conformation of serotonin 5-HT_{1A} receptor in complex with aripiprazole (PDB ID: 7E2Z) [53] and inactive state of serotonin 5-HT_{2A} receptor in complex with antagonist risperidone (PDB ID: 6A93) [54]. Protein structures were downloaded from the PDB database and modified by introducing necessary mutations and adding missing amino acid residues in extracellular loops. Then the receptor structures were subjected to preprocessing with the use of Protein Preparation Wizard of Schrödinger suite [55,56], as previously reported [57].

Grids were created based on co-crystallized ligands. The hydroxy groups of the following amino acids were flexible for molecular docking: Ser 121 (3.39), Ser 193 (5.43), Ser 197, Ser 409 (7.35), Tyr 408 (7.34), Tyr 416 (7.42), Thr 119 (3.37) and Thr 412 (7.38) for D_2

receptor, Ser 199 (5.43), Tyr 96 (2.63), Tyr 390 (7.42), Thr 121 (3.37), Thr 188, Thr 200 (5.44) and Thr 379 (7.31) for 5-HT_{1A} receptor, and Ser 131 (2.60), Ser 159 (3.36), Ser 242, Tyr 139, Tyr 370 (7.42), Thr 134 (2.63) and Thr 160 (3.37) for 5-HT_{2A} receptor. Ligands were subjected to molecular docking in Glide module [58] of Schrödinger suite of software, applying Standard precision (SP) method. 50 poses were generated for each ligand-receptor complex. The selection of final poses was made based on docking scores of Glide module and visual assessment. The results of molecular modeling were visualized using Maestro environment of Schrödinger suite [59].

4.5. X-ray studies

Single-crystal X-ray measurements were carried out at 100(2) K using an Oxford Diffraction Xcalibur CCD diffractometer equipped with a molybdenum sealed X-ray tube (MoK_α radiation, λ = 0.71073 Å) and a graphite monochromator. The CrysAlis [60] suite of programs was used for data collection, integration and data reduction. A multi-scan absorption correction was applied. The crystal structure was solved by direct method using SHELXS-2018 and the full-matrix least squares refinement was performed with the use of the SHELXL-2018 [61] (both operating under WinGX [62]). The nitrogen-bound hydrogen atoms were located from the different Fourier maps and refined isotropically while the H-atoms attached to carbon were positioned geometrically and refined using a riding model with $U_{iso}(H) = 1.2U_{eq}(C)$. Details of the X-ray crystal data structure determination and refinement are provided in Table S1 (see Supplementary Information). The molecular structures of compounds were drawn with ORTEP3 for Windows [62] and their molecular packing projections were prepared in Mercury [63]. The geometrical calculations were performed using the PLATON program [64]. The CIF file refinement can obtained free of charge from the Cambridge Crystallographic Data Center (CCDC) through www.ccdc.cam.ac.uk/data_request/cif.

4.6. ADMET parameters

4.6.1. Permeability profile

Pre-coated PAMPA Plate System Gentest from Corning (Tewksbury, MA, USA) was used in experiments according to manufacturer's instructions. Briefly, tested compound **11** and reference drugs were diluted in the PBS buffer (pH 7.4) to the final concentration 100 μM and added to a 96-well donor microplate. Following 5h of incubation at room temperature the exact quantity of molecules that penetrated from donor to acceptor wells through phospholipid membrane was estimated using the UPLC-MS spectrometry (Waters ACQUITY™ TQD system with the TQ Detector, Waters, Milford, USA). The permeability coefficients (P_e, cm/s) were calculated using the formula provided by the PAMPA Plate System vendor [34].

4.6.2. Influence on cytochrome P450 3A4 activity

Luminescence-based CYP3A4 P450-Glo kit, purchased from Promega® (Madison, WI, USA) was used to study the cytochrome activity. Experiments were conducted according to vendor's instructions and as described before [65]. Assays were performed twice in triplicates. The signal was measured using a microplate reader EnSpire PerkinElmer (Waltham, MA, USA).

4.6.3. Evaluation of neurotoxicity

Human neuroblastoma SH-SY5Y cell viability after 72 h of incubation with compound **11** and the reference cytostatic drugs: doxorubicin and paclitaxel was determined by performing the CellTiter 96 AQueous nonradioactive cell proliferation assay (Promega GmbH, Mannheim, Germany).

Cells were cultured in a 96-well plate at concentration of 5000 cells/well for 24 h before the tested compounds were added to the final concentrations of 0.3 to 30 μM. Following 3 days incubation period, the culture medium containing evaluated compounds was removed, and fresh

medium containing MTS dye–phenazine methosulfate solution was added to the cells. After 4 h of further incubation, the number of viable cells was determined by detection of formazan product of cell metabolic activity through the absorbance measurements at 490 nm directly from 96-well assay plates. Wells containing 1% DMSO were used as nontreated controls (fully viable cells) for calculations of the effects induced by tested compounds.

4.6.4. Interaction with P-glycoprotein

Ppg-Glo Assay Kit (Promega) was utilized to determine the influence of tested compounds on P-gp ATPase activity. The assay was conducted in accordance with the manufacturer's instructions. Verapamil was used as a reference substrate of P-gp, stimulating ATPase activity, whereas Na_3VO_4 was used as a reference blocker of ATPase activity.

Human P-gp membranes (25 µg/well) were incubated for 5 min at 37°C with tested compounds. Assay buffer containing dilution solvent – 1% DMSO was used as the negative control. After the preincubation period with tested compounds, P-gp ATPase reaction was started by the addition of enzyme substrate – MgATP (5 mM). The reaction was terminated after 40 minutes of incubation at 37°C and non-consumed ATP was quantified using ATP Detection Reagent provided with the kit. Assay plates were incubated at room temperature for additional 20 minutes in order to allow the luminescence signal to develop and were then analyzed using EnSpire Multiplate Reader (PerkinElmer).

4.6.5. *In vivo* PK/BBB permeability

Mice (see section 4.7.2. Animals) were injected with vehicle or compound **11** (40 mg/kg, ip) and decapitated in eight time points after administration (5 min, 15 min, 30 min, 1 h, 3 h, 6 h, 12 h and 24 h). The blood was collected into test tubes filled with anticoagulant (EDTA). Subsequently, samples were centrifuged at 3000 rpm for 10 min at + 4°C. Collected plasma was frozen and stored at -80°C. For the determination of a blood to plasma ratio, whole

blood and plasma was immediately used for the analysis. Partitioning of compound **11** within the blood was evaluated at 0.2 μg/mL; the protocol by Yu *et al.* [66] was employed. Concentration of compound **11** in plasma (C_p) and brain (C_{br}) was determined by liquid chromatography-mass spectrometry (Agielent Technologies 1290 Infinity II HPLC coupled to Agilent Technologies 6470 QQQ LC/MS). The brain uptake K_{in} was calculated as the quotient of C_{br}/AUC_{T0}, where AUC_{T0} is the area under the curve for plasma concentration from time 0 to time *T*.

4.7. Behavioral studies

4.7.1. Drugs

Compound **11** was dissolved in DMSO (final concentration of 0.5%), and then diluted by aqueous solution of 0.5% methylcellulose (MC). Compound **11** was administered intraperitoneally (i.p.), at the doses of 20, 40 or 80 mg/kg (detailed dose regimen is presented in the subsection for each experiment). D-amphetamine was dissolved in saline and injected subcutaneously (s.c.) at the dose of 5 mg/kg, based on our previous studies [17,45,67,68]. Each drug and vehicle were freshly prepared before each experiment. Control groups received vehicle injections at the same volume and by the same route of administration (i.p. or s.c., at the volume of 10 ml/kg).

4.7.2. Animals

The experiments were carried out on naive Swiss male mice (8 weeks old, weighing 20-30 g) obtained from the Centre of Experimental Medicine of the Medical University of Lublin. The animals were kept under standard laboratory conditions (12-h light/dark cycle, lights on 8.00 a.m., room temperature of 21 ± 1 °C, relative humidity of 50 ± 5%) with free access to tap water and a laboratory chow (Agropol, Poland). Animals were housed in groups of 4-5 per cage. All experiments were carried out between 8.30 a.m. and 2 p.m. All experiments were carried out according to the National Institute of Health Guidelines for the Care and Use of

Laboratory Animals and the European Community Council Directive for Care and Use of Laboratory Animals (2010/63/EU) and approved by the local ethics committee (permission number: 147/2018).

4.7.3. Motor coordination

To assess the impact of compound **11** on animals' motor coordination the Rota-rod test was used. This test has been validated in our laboratory and performed as previously described [17,67,68]. Briefly, mice were treated with compound **11** (20, 40 and 80 mg/kg, i.p.) or vehicle and, after 60 min, were placed on the rotarod apparatus. The time spent by each mouse on the Rota-rod was measured. Maximum time of testing after which the test ended was set for 3 min.

4.7.4. Spontaneous locomotor activity

To assess the impact of compound **11** on mice's locomotor activity, an animal activity meter Opto-Varimex-4 Auto-Track (Columbus Instruments, USA) was used. The animals' locomotion was measured by The Auto-Track System senses motion with a grid of infrared photocells. For the evaluation of spontaneous locomotor activity, animals were administered with compound **11** (20, 40 or 80 mg/kg, i.p.) or vehicle and, after 30 min, were placed in the apparatus for 30 min locomotion measurement. The distance traveled by each mouse was measured in cm ± SEM for each group.

Based on the results obtained in the locomotor activity test and Rota-rod test, the dose that displayed the most favorable profile and did not impaired animals' locomotion and motor coordination (e.i. 40 mg/kg) has been chosen for further behavioral studies.

4.7.5. Amphetamine-induced hyperactivity

To determine the impact of compound **11** on amphetamine-induced hyperactivity, the apparatus and method of measurement were identical to those used for spontaneous locomotor activity measurements. However, animals were first treated with compound **11** (40 mg/kg, i.p.)

or vehicle and after 30 min were injected with amphetamine (5 mg/kg, s.c.) and placed in the apparatus for 30 min measurement. This protocol has been previously validated in our laboratory [17,45,68].

4.7.6. Memory acquisition processes

To assess the impact of compound **11** on animals' memory performance the passive avoidance test was used. The PA apparatus consisted of a two-compartment acrylic box divided by a guillotine door. One compartment was illuminated with fluorescent light (8 W) and another was darkened. Both chambers had an electric grid floor. To assess the impact of compound **11** on the memory acquisition process, on Day 1 animals were treated with **11** (40 mg/kg, i.p.) or vehicle and, after 60 min, were placed into the light compartment of the PA apparatus. After 30s habituation time, the guillotine door was opened and the entrance of the mouse to the darkened box was punished by an electric foot shock (0.2 mA for 2 s). The time after which the mouse entered the darkened compartment was measured as TL1. On Day 2 (24h later) animals did not receive any injections and were placed into the light compartment of the apparatus. The time after which the mouse entered the darkened compartment was measured as TL2. The latency index (IL) was calculated for each animal: [IL = (TL2–TL1)/TL1] as the difference between retention and training latency times. An increase in the latency index has been interpreted as an improvement in the memory acquisition process.

4.7.7. Anxiety-like behavior

To assess the impact of compound **11** on animals' anxiety level the EPM was used. The EPM apparatus was made of plexiglass and consisted of four crossed arms forming a plus sign, raised 38.5 cm above the floor, and illuminated by a weak red light. Two arms were open (30 × 5 cm) and two enclosed (30 × 5 × 15 cm). The arms are extended from a central platform of 5 × 5 cm. Mice were treated with compound **11** (40 mg/kg, i.p.) or vehicle and, after 60 min, were tested in the EPM. Each mouse was individually placed at the central square of the plus-

maze apparatus, facing the open arm, and the behavior was observed for 5 min (by a treatment-blind observer, using a stopwatch totalizer). Specifically, the number of entries and the time spent in the open and enclosed arms were measured. The entry into one arm was defined as the stage when the animal placed all four paws past the line that divided the central square from the open arms. Time spent in open arms and number of entries into open arms were calculated as percentages. An anxiolytic effect was interpreted as an increase in the time spent in the open arms or/and in the number of entries into the open arms.

Figure captions

Table captions

Author contributions

P.S.: performed synthesis of the majority of reported compounds, molecular modeling, *in vitro* and behavioral studies, analyzed SAR, wrote the manuscript; K. M. T.-D.: performed and supervised behavioral studies, wrote the manuscript; A. L. M.: performed data analysis of *in vitro* studies; A. Z.: performed *in vitro* studies; O. W.-D.: performed behavioral studies and *in vivo* PK studies, wrote the manuscript; M. Z. W.: performed preliminary synthesis study; A. B.: performed X-ray studies, wrote the manuscript; A. T.: performed LC/MS analyzes, wrote the manuscript; T. M. W.: analyzed NMR spectra, supervised synthesis; A. C.: performed preliminary synthesis study; K. M. performed preliminary synthesis study; T. K.: performed ADMET assays, wrote the manuscript; K. S.: performed ADMET assays; M. I. L.: acquired funding; B. B.: performed and supervised behavioral studies and *in vivo* PK studies; J. T.: supervised synthesis; J. H.: supervised ADMET assays; E. F.: supervised and analyzed LC/MS studies, wrote the manuscript; E. P.: supervised *in vivo* PK studies; M. C.: supervised and analyzed *in vitro* studies, acquired funding, wrote the manuscript; A. A. K.: designed the study,

supervised molecular modeling, acquired funding. All authors also read and revised the manuscript.

Acknowledgments

The research was performed under the OPUS grant from National Science Center (NCN, Poland), grant number 2017/27/B/NZ7/01767 (to A.A.K). Calculations were partially performed under a computational grant by Interdisciplinary Center for Mathematical and Computational Modeling (ICM), Warsaw, Poland, grant number G85-948 (to A.A.K.). *In vitro* pharmacology assays were performed with support from the Spanish Ministry of Economy and Competitiveness (MINECO) (grant number PID2020-119754GB-I00 to M.C.). The study was also supported in part by an internal PB grant for PhD students (Medical University of Lublin, Poland) in terms of *in vivo* studies, grant number PBsd21 (to P.S.). Preliminary synthesis was partially performed with support from the Medical University of Warsaw student mini-grant number FW26/NM1/16/16. M. C. acknowledges technical assistance from Borja Blanco Babarro, with financial support from European Union-NextGenerationEU (Programa Investigo 2022, XUNTA de Galicia).

Conflict of interest

The authors declare no conflict of interest.

Data availability statement

The data that support the findings of this study are available in the Supplementary Information of this article.

References

[1] W.W. Fleischhacker, C. Arango, P. Arteel, T.R.E. Barnes, W. Carpenter, K. Duckworth, S. Galderisi, L. Halpern, M. Knapp, S.R. Marder, M. Moller, N. Sartorius, P. Woodruff, Schizophrenia--time to commit to policy change, Schizophr. Bull. 40 Suppl 3 (2014) S165-194. https://doi.org/10.1093/schbul/sbu006.

[2] S.R. Marder, T.D. Cannon, Schizophrenia, N. Engl. J. Med. 381 (2019) 1753–1761. https://doi.org/10.1056/NEJMra1808803.

[3] M.P. van den Heuvel, O. Sporns, G. Collin, T. Scheewe, R.C.W. Mandl, W. Cahn, J. Goñi, H.E. Hulshoff Pol, R.S. Kahn, Abnormal rich club organization and functional brain dynamics in schizophrenia, JAMA Psychiatry. 70 (2013) 783–792. https://doi.org/10.1001/jamapsychiatry.2013.1328.

[4] O.D. Howes, S. Kapur, The dopamine hypothesis of schizophrenia: version III--the final common pathway, Schizophr. Bull. 35 (2009) 549–562. https://doi.org/10.1093/schbul/sbp006.

[5] P.M. Haddad, C.U. Correll, The acute efficacy of antipsychotics in schizophrenia: a review of recent meta-analyses, Ther. Adv. Psychopharmacol. 8 (2018) 303–318. https://doi.org/10.1177/2045125318781475.

[6] D.G. Cunningham Owens, A Guide to the Extrapyramidal Side-Effects of Antipsychotic Drugs, 2nd ed., Cambridge University Press, Cambridge, 2014. https://doi.org/10.1017/CBO9781139149112.

[7] P. Stępnicki, M. Kondej, A.A. Kaczor, Current Concepts and Treatments of Schizophrenia, Mol. Basel Switz. 23 (2018) 2087. https://doi.org/10.3390/molecules23082087.

[8] J.M. Kane, O. Agid, M.L. Baldwin, O. Howes, J.-P. Lindenmayer, S. Marder, M. Olfson, S.G. Potkin, C.U. Correll, Clinical Guidance on the Identification and Management of

Treatment-Resistant Schizophrenia, J. Clin. Psychiatry. 80 (2019) 18com12123. https://doi.org/10.4088/JCP.18com12123.

[9] H. Elkis, Treatment-resistant schizophrenia, Psychiatr. Clin. North Am. 30 (2007) 511–533. https://doi.org/10.1016/j.psc.2007.04.001.

[10] J. Kane, G. Honigfeld, J. Singer, H. Meltzer, Clozapine for the treatment-resistant schizophrenic. A double-blind comparison with chlorpromazine, Arch. Gen. Psychiatry. 45 (1988) 789–796. https://doi.org/10.1001/archpsyc.1988.01800330013001.

[11] D. Siskind, L. McCartney, R. Goldschlager, S. Kisely, Clozapine v. first- and second-generation antipsychotics in treatment-refractory schizophrenia: systematic review and meta-analysis, Br. J. Psychiatry J. Ment. Sci. 209 (2016) 385–392. https://doi.org/10.1192/bjp.bp.115.177261.

[12] S. Jauhar, M. Johnstone, P.J. McKenna, Schizophrenia, The Lancet. 399 (2022) 473–486. https://doi.org/10.1016/S0140-6736(21)01730-X.

[13] M. Kondej, P. Stępnicki, A.A. Kaczor, Multi-Target Approach for Drug Discovery against Schizophrenia, Int. J. Mol. Sci. 19 (2018) 3105. https://doi.org/10.3390/ijms19103105.

[14] P. Stępnicki, M. Kondej, O. Koszła, J. Żuk, A.A. Kaczor, Multi-targeted drug design strategies for the treatment of schizophrenia, Expert Opin. Drug Discov. 16 (2021) 101–114. https://doi.org/10.1080/17460441.2020.1816962.

[15] S. Leucht, C. Corves, D. Arbter, R.R. Engel, C. Li, J.M. Davis, Second-generation versus first-generation antipsychotic drugs for schizophrenia: a meta-analysis, Lancet Lond. Engl. 373 (2009) 31–41. https://doi.org/10.1016/S0140-6736(08)61764-X.

[16] T. Pillinger, R.A. McCutcheon, L. Vano, Y. Mizuno, A. Arumuham, G. Hindley, K. Beck, S. Natesan, O. Efthimiou, A. Cipriani, O.D. Howes, Comparative effects of 18 antipsychotics on metabolic function in patients with schizophrenia, predictors of metabolic dysregulation, and association with psychopathology: a systematic review and

network meta-analysis, Lancet Psychiatry. 7 (2020) 64–77. https://doi.org/10.1016/S2215-0366(19)30416-X.

[17] A.A. Kaczor, K.M. Targowska-Duda, P. Stępnicki, A.G. Silva, O. Koszła, E. Kędzierska, A. Grudzińska, M. Kruk-Słomka, G. Biała, M. Castro, N-(3-{4-[3-(trifluoromethyl)phenyl]piperazin-1-yl}propyl)-1H-indazole-3-carboxamide (D2AAK3) as a potential antipsychotic: In vitro, in silico and in vivo evaluation of a multi-target ligand, Neurochem. Int. 146 (2021) 105016. https://doi.org/10.1016/j.neuint.2021.105016.

[18] K.G. Liu, A.J. Robichaud, A general and convenient synthesis of N-aryl piperazines, Tetrahedron Lett. 46 (2005) 7921–7922. https://doi.org/10.1016/j.tetlet.2005.09.092.

[19] R.V. Patel, B. Mistry, R. Syed, A.K. Rathi, Y.-J. Lee, J.-S. Sung, H.-S. Shinf, Y.-S. Keum, Chrysin-piperazine conjugates as antioxidant and anticancer agents, Eur. J. Pharm. Sci. 88 (2016) 166–177. https://doi.org/10.1016/j.ejps.2016.02.011.

[20] J.A. Ballesteros, H. Weinstein, Integrated methods for the construction of three-dimensional models and computational probing of structure-function relations in G protein-coupled receptors, in: S.C. Sealfon (Ed.), Methods Neurosci., Academic Press, 1995: pp. 366–428. https://doi.org/10.1016/S1043-9471(05)80049-7.

[21] C.R. Groom, I.J. Bruno, M.P. Lightfoot, S.C. Ward, The Cambridge Structural Database, Acta Crystallogr. Sect. B Struct. Sci. Cryst. Eng. Mater. 72 (2016) 171–179. https://doi.org/10.1107/S2052520616003954.

[22] F.H. Allen, D.G. Watson, L. Brammer, A.G. Orpen, R. Taylor, Typical interatomic distances: organic compounds, in: Int. Tables Crystallogr., American Cancer Society, 2006: pp. 790–811. https://doi.org/10.1107/97809553602060000621.

[23] F. Crestey, S. Stiebing, R. Legay, V. Collot, S. Rault, Design and synthesis of a new indazole library: direct conversion of N-methoxy-N-methylamides (Weinreb amides) to

3-keto and 3-formylindazoles, Tetrahedron. 63 (2007) 419–428. https://doi.org/10.1016/j.tet.2006.10.063.

[24] S. Kuang, P. Zhang, E.Z. Dong, G. Jennings, B. Zhao, M. Pierce, Crystal form control and particle size control of RG3487, a nicotinic α7 receptor partial agonist, Int. J. Pharm. 508 (2016) 109–122. https://doi.org/10.1016/j.ijpharm.2016.04.066.

[25] M.S.R. Murty, R.V. Rao, K.R. Ram, N.R. Reddy, J.S. Yadav, B. Sridhar, Zinc-Mediated Facile and Efficient Chemoselective S-Alkylation of 5-Aryl-1,3,4-oxadiazole-2-thiols in the Absence of Base, Synth. Commun. 40 (2010) 2914–2921. https://doi.org/10.1080/00397910903340660.

[26] C. Enguehard-Gueiffier, H. Hübner, A. El Hakmaoui, H. Allouchi, P. Gmeiner, A. Argiolas, M.R. Melis, A. Gueiffier, 2-[(4-Phenylpiperazin-1-yl)methyl]imidazo(di)azines as Selective D4-Ligands. Induction of Penile Erection by 2-[4-(2-Methoxyphenyl)piperazin-1-ylmethyl]imidazo[1,2-a]pyridine (PIP3EA), a Potent and Selective D4 Partial Agonist, J. Med. Chem. 49 (2006) 3938–3947. https://doi.org/10.1021/jm060166w.

[27] J. Kossakowski, E. Hejchman, I. Wolska, Synthesis and Structural Characterization of Aminoalkanol Derivatives of 2,3-Dihydro-2,2-dimethyl-7-benzofuranol with an Expected β-Adrenolytic and / or Anxiolytic Activity, Z. Für Naturforschung B. 57 (2002) 285–294. https://doi.org/10.1515/znb-2002-0305.

[28] Z.S. Şahin, M. Yarım, M. Köksal, Density functional computational and X-ray studies on pharmaceutical compound 1-{3-[4-(4-fluorophenyl)piperazin-1-yl]propyl}-1H-indole, Eur. J. Chem. 8 (2017) 1–7. https://doi.org/10.5155/eurjchem.8.1.1-7.1512.

[29] J. Bernstein, R.E. Davis, L. Shimoni, N.-L. Chang, Patterns in Hydrogen Bonding: Functionality and Graph Set Analysis in Crystals, Angew. Chem. Int. Ed. Engl. 34 (1995) 1555–1573. https://doi.org/10.1002/anie.199515551.

[30] D. Cremer, J.A. Pople, General definition of ring puckering coordinates, J. Am. Chem. Soc. 97 (1975) 1354–1358. https://doi.org/10.1021/ja00839a011.

[31] J.C.A. Boeyens, The conformation of six-membered rings, J. Cryst. Mol. Struct. 8 (1978) 317–320. https://doi.org/10.1007/BF01200485.

[32] C.A.G. Haasnoot, The conformation of six-membered rings described by puckering coordinates derived from endocyclic torsion angles, J. Am. Chem. Soc. 114 (1992) 882–887. https://doi.org/10.1021/ja00029a013.

[33] L. Di, E. Kerns, Drug-Like Properties: Concepts, Structure Design and Methods from ADME to Toxicity Optimization, 2nd edition, Academic Press, Amsterdam ; Boston, 2016.

[34] X. Chen, A. Murawski, K. Patel, C.L. Crespi, P.V. Balimane, A novel design of artificial membrane for improving the PAMPA model, Pharm. Res. 25 (2008) 1511–1520. https://doi.org/10.1007/s11095-007-9517-8.

[35] Y.-T. Liu, H.-P. Hao, C.-X. Liu, G.-J. Wang, H.-G. Xie, Drugs as CYP3A probes, inducers, and inhibitors, Drug Metab. Rev. 39 (2007) 699–721. https://doi.org/10.1080/03602530701690374.

[36] D.F.G. Hendriks, S.U. Vorrink, T. Smutny, S.C. Sim, Å. Nordling, S. Ullah, M. Kumondai, B.C. Jones, I. Johansson, T.B. Andersson, V.M. Lauschke, M. Ingelman-Sundberg, Clinically Relevant Cytochrome P450 3A4 Induction Mechanisms and Drug Screening in Three-Dimensional Spheroid Cultures of Primary Human Hepatocytes, Clin. Pharmacol. Ther. 108 (2020) 844–855. https://doi.org/10.1002/cpt.1860.

[37] C. Jones, D. Watson, K. Fone, Animal models of schizophrenia, Br. J. Pharmacol. 164 (2011) 1162–1194. https://doi.org/10.1111/j.1476-5381.2011.01386.x.

[38] M. Kołaczkowski, P. Mierzejewski, P. Bienkowski, A. Wesołowska, A. Newman-Tancredi, Antipsychotic, antidepressant, and cognitive-impairment properties of

antipsychotics: rat profile and implications for behavioral and psychological symptoms of dementia, Naunyn. Schmiedebergs Arch. Pharmacol. 387 (2014) 545–557. https://doi.org/10.1007/s00210-014-0966-4.

[39] G. Zhang, R.W. Stackman, The role of serotonin 5-HT2A receptors in memory and cognition, Front. Pharmacol. 6 (2015) 225. https://doi.org/10.3389/fphar.2015.00225.

[40] D.H. Overstreet, R.C. Commissaris, R. De La Garza, S.E. File, D.J. Knapp, L.S. Seiden, Involvement of 5-HT1A receptors in animal tests of anxiety and depression: evidence from genetic models, Stress Amst. Neth. 6 (2003) 101–110. https://doi.org/10.1080/1025389031000111311.

[41] L.K. Heisler, H.-M. Chu, T.J. Brennan, J.A. Danao, P. Bajwa, L.H. Parsons, L.H. Tecott, Elevated anxiety and antidepressant-like responses in serotonin 5-HT1A receptor mutant mice, Proc. Natl. Acad. Sci. U. S. A. 95 (1998) 15049–15054.

[42] N. Andrews, S. Hogg, L.E. Gonzalez, S.E. File, 5-HT1A receptors in the median raphe nucleus and dorsal hippocampus may mediate anxiolytic and anxiogenic behaviours respectively, Eur. J. Pharmacol. 264 (1994) 259–264. https://doi.org/10.1016/0014-2999(94)00473-0.

[43] J. Selent, M. Marti-Solano, J. Rodríguez, P. Atanes, J. Brea, M. Castro, F. Sanz, M.I. Loza, M. Pastor, Novel insights on the structural determinants of clozapine and olanzapine multi-target binding profiles, Eur. J. Med. Chem. 77 (2014) 91–95. https://doi.org/10.1016/j.ejmech.2014.02.058.

[44] K.A. Berg, S. Maayani, J. Goldfarb, C. Scaramellini, P. Leff, W.P. Clarke, Effector pathway-dependent relative efficacy at serotonin type 2A and 2C receptors: evidence for agonist-directed trafficking of receptor stimulus, Mol. Pharmacol. 54 (1998) 94–104.

[45] A.A. Kaczor, K.M. Targowska-Duda, A.G. Silva, M. Kondej, G. Biała, M. Castro, N-(2-Hydroxyphenyl)-1-[3-(2-oxo-2,3-dihydro-1H- benzimidazol-1-yl)propyl]piperidine-4-

Carboxamide (D2AAK4), a Multi-Target Ligand of Aminergic GPCRs, as a Potential Antipsychotic, Biomolecules. 10 (2020) 349. https://doi.org/10.3390/biom10020349.

[46] A.A. Kaczor, A.G. Silva, M.I. Loza, P. Kolb, M. Castro, A. Poso, Structure-Based Virtual Screening for Dopamine D2 Receptor Ligands as Potential Antipsychotics, ChemMedChem. 11 (2016) 718–729. https://doi.org/10.1002/cmdc.201500599.

[47] E. Magli, B. Severino, A. Corvino, E. Perissutti, F. Frecentese, I. Saccone, F. Giordano, M. Castro, J. Brea, M.I. Loza, V. Santagada, G. Caliendo, F. Fiorino, New Serotoninergic Ligands Containing Indolic and Methyl Indolic Nuclei: Synthesis and In Vitro Pharmacological Evaluation, Med. Chem. 16 (2020) 517–530. https://doi.org/10.2174/1573406415666190613153220.

[48] P. Leff, I.G. Dougall, Further concerns over Cheng-Prusoff analysis, Trends Pharmacol. Sci. 14 (1993) 110–112. https://doi.org/10.1016/0165-6147(93)90080-4.

[49] Schrödinger Release 2021–4: LigPrep, Schrödinger, LLC, New York, NY, 2021.

[50] Schrödinger Release 2021–4: Epik, Schrödinger, LLC, New York, NY, 2021.

[51] J.R. Greenwood, D. Calkins, A.P. Sullivan, J.C. Shelley, Towards the comprehensive, rapid, and accurate prediction of the favorable tautomeric states of drug-like molecules in aqueous solution, J. Comput. Aided Mol. Des. 24 (2010) 591–604. https://doi.org/10.1007/s10822-010-9349-1.

[52] S. Wang, T. Che, A. Levit, B.K. Shoichet, D. Wacker, B.L. Roth, Structure of the D2 dopamine receptor bound to the atypical antipsychotic drug risperidone, Nature. 555 (2018) 269–273. https://doi.org/10.1038/nature25758.

[53] P. Xu, S. Huang, H. Zhang, C. Mao, X.E. Zhou, X. Cheng, I.A. Simon, D.-D. Shen, H.-Y. Yen, C.V. Robinson, K. Harpsøe, B. Svensson, J. Guo, H. Jiang, D.E. Gloriam, K. Melcher, Y. Jiang, Y. Zhang, H.E. Xu, Structural insights into the lipid and ligand

regulation of serotonin receptors, Nature. 592 (2021) 469–473. https://doi.org/10.1038/s41586-021-03376-8.

[54] K.T. Kimura, H. Asada, A. Inoue, F.M.N. Kadji, D. Im, C. Mori, T. Arakawa, K. Hirata, Y. Nomura, N. Nomura, J. Aoki, S. Iwata, T. Shimamura, Structures of the 5-HT2A receptor in complex with the antipsychotics risperidone and zotepine, Nat. Struct. Mol. Biol. 26 (2019) 121–128. https://doi.org/10.1038/s41594-018-0180-z.

[55] Schrödinger Release 2021-4: Protein Preparation Wizard, Schrödinger, LLC, New York, NY, 2021.

[56] G. Madhavi Sastry, M. Adzhigirey, T. Day, R. Annabhimoju, W. Sherman, Protein and ligand preparation: parameters, protocols, and influence on virtual screening enrichments, J. Comput. Aided Mol. Des. 27 (2013) 221–234. https://doi.org/10.1007/s10822-013-9644-8.

[57] J.Z. Patel, T. Parkkari, T. Laitinen, A.A. Kaczor, S.M. Saario, J.R. Savinainen, D. Navia-Paldanius, M. Cipriano, J. Leppänen, I.O. Koshevoy, A. Poso, C.J. Fowler, J.T. Laitinen, T. Nevalainen, Chiral 1,3,4-Oxadiazol-2-ones as Highly Selective FAAH Inhibitors, J. Med. Chem. 56 (2013) 8484–8496. https://doi.org/10.1021/jm400923s.

[58] Schrödinger Release 2021–4: Glide, Schrödinger, LLC, New York, NY, 2021., (n.d.).

[59] Schrödinger Release 2021–4: Maestro, Schrödinger, LLC, New York, NY, 2021., (n.d.).

[60] CrysAlis PRO., (2014).

[61] G.M. Sheldrick, Crystal structure refinement with SHELXL, Acta Crystallogr. Sect. C Struct. Chem. 71 (2015) 3–8. https://doi.org/10.1107/S2053229614024218.

[62] L.J. Farrugia, WinGX and ORTEP for Windows: an update, J. Appl. Crystallogr. 45 (2012) 849–854. https://doi.org/10.1107/S0021889812029111.

[63] C.F. Macrae, I. Sovago, S.J. Cottrell, P.T.A. Galek, P. McCabe, E. Pidcock, M. Platings, G.P. Shields, J.S. Stevens, M. Towler, P.A. Wood, Mercury 4.0: from visualization to

analysis, design and prediction, J. Appl. Crystallogr. 53 (2020) 226–235. https://doi.org/10.1107/S1600576719014092.

[64] A.L. Spek, Single-crystal structure validation with the program PLATON, J. Appl. Crystallogr. 36 (2003) 7–13. https://doi.org/10.1107/S0021889802022112.

[65] K. Szczepańska, S. Pockes, S. Podlewska, C. Höring, K. Mika, G. Latacz, M. Bednarski, A. Siwek, T. Karcz, M. Nagl, M. Bresinsky, D. Mönnich, U. Seibel, K.J. Kuder, M. Kotańska, H. Stark, S. Elz, K. Kieć-Kononowicz, Structural modifications in the distal, regulatory region of histamine H3 receptor antagonists leading to the identification of a potent anti-obesity agent, Eur. J. Med. Chem. 213 (2021) 113041. https://doi.org/10.1016/j.ejmech.2020.113041.

[66] S. Yu, S. Li, H. Yang, F. Lee, J.-T. Wu, M.G. Qian, A novel liquid chromatography/tandem mass spectrometry based depletion method for measuring red blood cell partitioning of pharmaceutical compounds in drug discovery, Rapid Commun. Mass Spectrom. RCM. 19 (2005) 250–254. https://doi.org/10.1002/rcm.1777.

[67] A.A. Kaczor, K.M. Targowska-Duda, B. Budzyńska, G. Biała, A.G. Silva, M. Castro, In vitro, molecular modeling and behavioral studies of 3-{[4-(5-methoxy-1H-indol-3-yl)-1,2,3,6-tetrahydropyridin-1-yl]methyl}-1,2-dihydroquinolin-2-one (D2AAK1) as a potential antipsychotic, Neurochem. Int. 96 (2016) 84–99. https://doi.org/10.1016/j.neuint.2016.03.003.

[68] M. Kondej, T.M. Wróbel, K.M. Targowska-Duda, A. Leandro Martínez, O. Koszła, P. Stępnicki, A. Zięba, A. Paz, O. Wronikowska-Denysiuk, M.I. Loza, M. Castro, A.A. Kaczor, Multitarget Derivatives of D2AAK1 as Potential Antipsychotics: The Effect of Substitution in the Indole Moiety, ChemMedChem. 17 (2022) e202200238. https://doi.org/10.1002/cmdc.202200238.